JOURNAL OF COMPUTATIONAL PHYSICS 20, 442–479 (1976)

A Mixed Spectral and Finite Difference Model to Study Baroclinic Annulus Waves*

CHARLES QUON

Geophysical Fluid Dynamics Institute, Florida State University, and Bedford Institute of Oceanography, Nova Scotia, Canada

Received June 19, 1975

A mixed spectral and finite difference model to study finite amplitude baroclinic waves in a differentially heated rotating annulus is presented. The model consists of the full Navier–Stokes equations and the heat equation. The field variables $\mathbf{f} = \mathbf{f}(r, \phi, z; t)$ are decomposed into zonally averaged components $\mathbf{f}_0(r, z; t)$ and eddy components $\mathbf{f}'(r, \phi, z; t)$, the latter being periodic in ϕ and represented in terms of Fourier series. The unknowns $\mathbf{f}_0(r, z; t)$ and $\mathbf{f}^{c,s}(r, z; t)$, which are Fourier amplitudes of $\mathbf{f}'(r, \phi, z; t)$ are governed by two-dimensional primitive equations with the addition of source terms. These equations are solved semi-implicitly by the alternating direction implicit method on variable grids.

A simplified model with two Fourier components which permits self-interaction of the chosen wave and the interaction of the wave and the mean fields had been used to repeat a computation done by G. P. Williams, who used a fully three-dimensional finite difference algorithm. We can reproduce almost all of Williams' results in 1/20 of the computing time with the present model. It only requires 1/30 the additional computer storage of Williams' finite difference model over the axisymmetric problem.

The potential of the present model for investigation of multiwave interaction as well as the advantages and disadvantages of the two different approaches is discussed.

1. INTRODUCTION

Hide [8] and Fultz [5] showed that when the side walls of a vertical rotating annulus of fluid are differentially heated, one of four distinct states of flow will arise, depending on the imposed rotation rate and temperature differential: (1) axisymmetric flow, (2) turbulence, (3) steady waves, and (4) unsteady waves. In this paper, an efficient numerical algorithm to study the development and structure of finite amplitude annulus waves is presented.

Two algorithms have been developed to study this particular problem. Williams [23, 24] used a three-dimensional finite difference scheme to study an annulus wave of azimuthal wavenumber 5. Dietrich [2] used an algorithm based on Galerkin's technique to study baroclinic flows in a rotating, differentially heated straight

*Geophysical Fluid Dynamics Institute Contribution No. 115; a Bedford Institute Contribution.

Copyright © 1976 by Academic Press, Inc.
All rights of reproduction in any form reserved.

channel with a rigid lid (a narrow gap approximation of the annulus). Making use of the simple channel geometry, he was able to exploit symmetry to reduce the total amount of computation.

Why, then, a third algorithm to accomplish a task that has apparently been resolved by two authors? Dietrich's approach works well for his channel model, but it is not clear how efficiently it will work in an annulus geometry. Williams' three-dimensional finite difference scheme is inefficient for several reasons: (1) It requires very large computer storage since it is a fully three-dimensional system in space that also requires storage of variables on two time levels. The model presented here reduced the storage requirement by (a) using a scheme with one time level, and (b) transforming the system into a larger one but with only two independent spatial variables. (2) Williams' scheme is completely explicit; therefore, the time step is very much limited by the diffusive time scale. If the diffusive terms are treated implicitly or semi-implicitly one can use larger time steps. (3) The odd and even time steps diverge in Williams' computation. This divergence can also be eliminated by using an implicit or other appropriate schemes. (4) Constant grids are inefficient for boundary layer flow. Variable grids are more economical.

Furthermore, it is well known that the annulus waves are very regular and have distinct wavenumbers in the azimuthal direction. The most intriguing question is whether one can fully exploit this characteristic and simulate a three-dimensional annulus wave using only one dominant spectral component in the algorithm. If this can be accomplished, one could extend the model to study the interactions of a number of waves, and hopefully, other more complicated phenomena.

2. Formulation of the Problem

Let us consider an annulus of standard geometry with inner radius r_0 outer radius r_1, and height H, as shown in Fig. 1. The annulus has perfectly conducting outer and inner walls, which are to be maintained at constant temperatures $T_0 \pm \Delta T/2$, and is filled with an incompressible fluid of kinematic viscosity ν and thermometric conductivity κ. The whole system rotates about its vertical axis at an angular velocity $\Omega\hat{k}$, antiparallel to gravity $-g\hat{k}$. Then the governing equations of the fluid in the rotating frame of reference with Boussinesq approximation are

$$\frac{D}{Dt}\mathbf{V} + 2\Omega\hat{k} \times \mathbf{V} = -\frac{1}{\rho^{(0)}}\nabla p - \frac{\rho}{\rho^{(0)}}\left(g\hat{k} - \frac{1}{2}\Omega^2\nabla \mid \hat{k} \times \mathbf{r} \mid^2\right) - \nu\nabla \times \nabla \times \mathbf{V},$$

$$\nabla \cdot \mathbf{V} = 0,$$

$$(D/Dt)\, T = \kappa\nabla^2 T,$$

$$\rho = \rho^{(0)}\{1 - \alpha(T - T^{(0)})\},$$

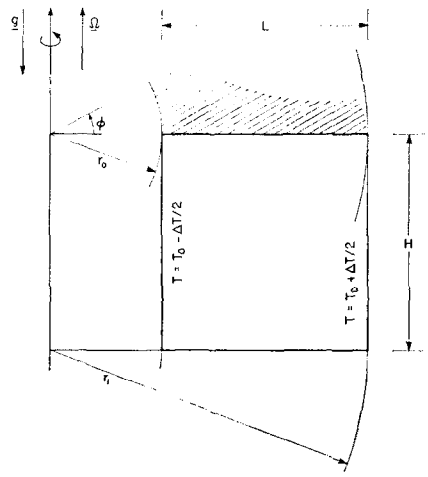

FIG. 1. The physical system.

where $\mathbf{V}$ is the velocity vector, p is the pressure, ρ is the density, which depends linearly on T, the temperature of the fluid; all are functions of the position vector $\mathbf{r}$, and time t. $T^{(0)}$ and $\rho^{(0)}$ are the reference temperature and the corresponding density of the fluid.

The centrifugal term $\Omega^2\nabla \mid \hat{k} \times \mathbf{r} \mid^2$ will be neglected under the formal condition that $\Omega^2 r/g \ll 1$. The neglect of this term is necessary in order to be consistent with the neglect of curvature on a free surface, although the term may have a noticeable effect in the lower transition region where Ω is large [12].

For computational convenience, the above equations in cylindrical polar coordinates (r, ϕ, z) are nondimensionalized as follows, where (*) denotes nondimensional parameters.

$$\begin{aligned}
\mathbf{V} &= (2\Omega L)\,\mathbf{V}^*, \qquad t = (2\Omega)^{-1} t^*, \qquad \mathbf{r} = L\mathbf{r}^*, \\
P^* &= \{(p - p^{(0)})\,\rho^{(0)} + gz(1 + \alpha T^{(0)})\}(2\Omega L)^{-2}, \\
T &= T^{(0)} + \Delta T \cdot T^*, \\
L &= (r_1 - r_0),
\end{aligned}$$

where $p^{(0)}$ represents some constant surface pressure.

In flux form the equations for the nondimensional velocity components (u^*, v^*, w^*) and temperature T^* are (with * dropped)

$$\begin{aligned}
&\frac{\partial}{\partial t} u + \frac{1}{r}\frac{\partial}{\partial r}(ru^2) + \frac{1}{r}\frac{\partial}{\partial \phi}(uv) + \frac{\partial}{\partial z}(uw) - \left(1 + \frac{v}{r}\right) v \\
&\quad = -\frac{\partial p}{\partial r} + \epsilon\left(\nabla^2 u - \frac{u}{r^2} - \frac{2}{r^2}\frac{\partial v}{\partial \phi}\right), \qquad (1)
\end{aligned}$$

$$\frac{\partial}{\partial t} v + \frac{1}{r}\frac{\partial}{\partial r}(ruv) + \frac{1}{r}\frac{2}{\partial\phi} v^2 + \frac{\partial}{\partial z}(wv) + \left(1 + \frac{v}{r}\right) u$$
$$= -\frac{1}{r}\frac{\partial p}{\partial \phi} + \epsilon\left(\nabla^2 v - \frac{v}{r^2} + \frac{2}{r^2}\frac{\partial u}{\partial \phi}\right), \tag{2}$$

$$\frac{\partial}{\partial t} w + \frac{1}{r}\frac{\partial}{\partial r}(ruw) + \frac{1}{r}\frac{\partial}{\partial \phi}(vw) + \frac{\partial}{\partial z} w^2 = -\frac{\partial p}{\partial z} + \beta T + \epsilon\nabla^2 w, \tag{3}$$

$$\frac{\partial}{\partial t} T + \frac{1}{r}\frac{\partial}{\partial r}(ruT) + \frac{1}{r}\frac{\partial}{\partial \phi}(vT) + \frac{\partial}{\partial z}(wT) = \frac{\epsilon}{\sigma}\nabla^2 T, \tag{4}$$

$$(1/r)(\partial/\partial r)(ru) + (1/r)(\partial v/\partial\phi) + (\partial/\partial z)\, w = 0. \tag{5}$$

The boundary conditions are

$$\begin{aligned} u = v = w &= 0 && \text{at } r = A_2,\ 1 + A_2 \text{ and } z = 0,\\ \partial u/\partial z = \partial v/\partial z &= w = 0 && \text{at } z = A_1,\\ T &= \pm\tfrac{1}{2} && \text{at } r = 1 + A_2,\\ & && \quad = A_2,\\ \partial T/\partial z &= 0 && \text{at } z = 0, A_1, \end{aligned} \tag{6}$$

where

$$A_1 = H/L, \qquad 0 \leqslant z \leqslant A_1,$$
$$A_2 = r_0/L, \qquad A_2 \leqslant r \leqslant 1 + A_2.$$

The nondimensional parameters are

$\epsilon = \nu/(2\Omega L^2)$, the Ekman number,
$\beta = \alpha g\, \Delta T/(4\Omega^2 L)$, the thermal Rossby number,
$\sigma = \nu/\kappa$, the Prandtl number.

They specify the Rayleigh number $= \alpha g\, \Delta T\, H^3/(\kappa\nu) = \sigma\beta\epsilon^{-2} \cdot A_1^3$, which is reduced to $\sigma\beta\epsilon^{-2}$ when $A_1 = 1$ as used later in this paper. One nondimensional period of rotation is equal to 4π. The Rossby number $U/(2\Omega L)$ is equivalent to the largest nondimensional azimuthal velocity v of the final result.

3. The Mean Field and Fourier Amplitude Equations

We shall decompose the field variables $\mathbf{f} = (u, v, w, T, p)$ into two parts:

$$\mathbf{f} = \mathbf{f}_0(r, z; t) + \mathbf{f}'(r, \phi, z; t), \tag{7}$$

where $\mathbf{f}_0$ is a mean field vector. It is defined as

$$\mathbf{f}_0 = (1/2\pi) \int_0^{2\pi} \mathbf{f}\, d\phi = (u_0\,, v_0\,, w_0\,, T_0\,, p_0). \tag{8a}$$

$\mathbf{f}'$ is not necessarily small but is periodic in ϕ. Hence, it can be further decomposed into Fourier components as follows.

$$\mathbf{f}'(r, \phi, z; t) = \sqrt{2} \sum_k \{\mathbf{f}_k{}^c(r, z; t) \cos k\phi + \mathbf{f}_k{}^s(r, z; t) \sin k\phi\}, \tag{8b}$$

where

$$\mathbf{f}_k{}^c = (u_k{}^c, v_k{}^c, w_k{}^c, T_k{}^c, p_k{}^c), \tag{8c}$$

$$\mathbf{f}_k{}^s = (u_k{}^s, v_k{}^s, w_k{}^s, T_k{}^s, p_k{}^s), \tag{8d}$$

which are consistent with (8a).

If we substitute (7) into Eqs. (1)–(5) and integrate these with respect to ϕ from 0 to 2π, we obtain the mean field equations

$$\begin{aligned}
&\frac{\partial u_0}{\partial t} + \frac{1}{r}\frac{\partial}{\partial r}(r u_0{}^2) + \frac{\partial}{\partial z}(u_0 w_0) - \epsilon(\tilde{\nabla}^2 u_0 - u_0/r^2) \\
&\quad = -\frac{\partial p_0}{\partial r} + \left(1 + \frac{v_0}{r}\right) v_0 - \frac{1}{r}\frac{\partial}{\partial r}\sum_\kappa (r(u_\kappa{}^c)^2 + r(u_\kappa{}^s)^2) \\
&\qquad - \frac{\partial}{\partial z}\sum_\kappa (u_\kappa{}^c w_\kappa{}^c + u_\kappa{}^s w_\kappa{}^s) + \frac{1}{r}\sum_\kappa ((v_\kappa{}^c)^2 + (v_\kappa{}^s)^2),
\end{aligned} \tag{9}$$

$$\begin{aligned}
&\frac{\partial v_0}{\partial t} + \frac{1}{r}\frac{2}{\partial r}(r u_0 v_0) + \frac{\partial}{\partial z}(w_0 v_0) - \epsilon\left(\tilde{\nabla}^2 v_0 - \frac{v_0}{r^2}\right) \\
&= -\left(1 + \frac{v_0}{r}\right) u_0 - \frac{1}{r}\frac{\partial}{\partial r}\sum_\kappa (r u_\kappa{}^c v_\kappa{}^c + r u_\kappa{}^s v_\kappa{}^s) \\
&\qquad \frac{\partial}{\partial z}\sum_\kappa (w_\kappa{}^c v_\kappa{}^c + w_\kappa{}^s v_\kappa{}^s) - \frac{1}{r}\sum_\kappa (u_\kappa{}^c v_\kappa{}^c + u_\kappa{}^s v_\kappa{}^s),
\end{aligned} \tag{10}$$

$$\begin{aligned}
&\frac{\partial w_0}{\partial t} + \frac{1}{r}\frac{\partial}{\partial r}(r u_0 w_0) + \frac{\partial}{\partial z} w_0{}^2 - \epsilon\tilde{\nabla}^2 w_0 \\
&\quad = -\frac{\partial p_0}{\partial z} + \beta T_0 - \frac{1}{r}\frac{\partial}{\partial r}\sum_\kappa (r u_\kappa{}^c w_\kappa{}^c + r u_\kappa{}^s w_\kappa{}^s) \\
&\qquad - \frac{\partial}{\partial z}\sum_\kappa ((w_\kappa{}^c)^2 + (w_\kappa{}^s)^2),
\end{aligned} \tag{11}$$

$$\frac{\partial T_0}{\partial t} + \frac{1}{r}\frac{\partial}{\partial r}(ru_0T_0) + \frac{\partial}{\partial z}(w_0T_0) - \frac{\epsilon}{\sigma}\tilde{\nabla}^2 T_0$$
$$= -\frac{1}{r}\frac{\partial}{\partial r}\sum_\kappa (ru_\kappa{}^c T_\kappa{}^c + ru_\kappa{}^s T_\kappa{}^s) - \frac{\partial}{\partial z}\sum_\kappa (w_\kappa{}^c T_\kappa{}^c + w_\kappa{}^s T_\kappa{}^s), \tag{12}$$

$$(1/r)(\partial/\partial r)(ru_0) + (\partial/\partial z)\, w_0 = 0, \tag{13}$$

where $\tilde{\nabla}^2 = ((1/r)(\partial/\partial r)\, r(\partial/\partial r) + (\partial^2/\partial z^2))$ is two-dimensional Laplacian. The boundary conditions are the same as (6), where u, v, w, T, and P are replaced by u_0, v_0, w_0, T_0, and P_0.

To obtain the eddy amplitude equations, we again substitute (7) into Eqs. (1)–(5). The amplitude equations for wavenumber j are obtained by multiplying through the resulting equations by $\cos j\phi$ or $\sin j\phi$, and integrating them from 0 to 2π. The equations for the jth component are as follows.

$$\frac{\partial}{\partial t}u_j^{c,s} + \frac{1}{r}\frac{\partial}{\partial r}(ru_0u_j^{c,s}) + \frac{\partial}{\partial z}(w_0u_j^{c,s}) - \epsilon\left(\tilde{\nabla}^2 - \frac{(1+j^2)}{r^2}\right)u_j^{c,s}$$
$$= -\frac{\partial}{\partial r}p_j^{c,s} + \left(1 + \frac{2v_0}{r}\right)v_j^{c,s} \pm \epsilon\frac{2j}{r^2}v_j^{s,c}$$
$$- \left\{\frac{1}{r}\frac{\partial}{\partial r}(ru_0u_j^{c,s}) \pm \frac{j}{r}(v_0u_j^{s,c} + u_0v_j^{s,c})\right\}$$
$$+ \frac{\partial}{\partial z}(u_0w_j^{c,s}) + \mathcal{N}^{c,s}(u)_j, \tag{14a, b}$$

$$\frac{\partial}{\partial t}v_j^{c,s} + \frac{1}{r}\frac{\partial}{\partial r}(ru_0v_j^{c,s}) + \frac{\partial}{\partial z}(w_0v_j^{c,s}) - \epsilon\left(\tilde{\nabla}^2 - \frac{(1+j^2)}{r^2}\right)v_j^{c,s}$$
$$= \pm\frac{j}{r}p_j^{s,c} - \left(1 + \frac{v_0}{r}\right)u_j^{c,s} - \frac{u_0}{r}v_j^{c,s}$$
$$\pm\epsilon\frac{2j}{r}u_j^{s,c} - \left\{\frac{1}{r}\frac{\partial}{\partial r}(rv_0u_j^{c,s})\right.$$
$$\left.\pm\frac{2j}{r}v_0v_j^{s,c} + \frac{\partial}{\partial z}(v_0w_j^{c,s})\right\} + \mathcal{N}^{c,s}(v)_j, \tag{15a,b}$$

$$\frac{\partial}{\partial t}w_j^{c,s} + \frac{1}{r}\frac{\partial}{\partial r}(ru_0w_j^{c,s}) + \frac{\partial}{\partial z}(w_0w_j^{c,s}) - \epsilon\left(\tilde{\nabla}^2 - \frac{j^2}{r^2}\right)w_j^{c,s}$$
$$= -\frac{\partial}{\partial z}p_j^{c,s} + \beta T_j^{c,s} - \left\{\frac{1}{r}\frac{\partial}{\partial r}(rw_0{}_j^{c,s})\right.$$
$$\left.\pm\frac{j}{r}(v_0w_j^{s,c} + w_0v_j^{s,c}) + \frac{\partial}{\partial z}(w_0w_j^{c,s})\right\} + \mathcal{N}^{c,s}(w)_j, \tag{16a, b}$$

$$\frac{\partial}{\partial t} T_j^{c,s} + \frac{1}{r}\frac{\partial}{\partial r}(ru_0 T_j^{c,s}) + \frac{\partial}{\partial z}(w_0 T_j^{c,s}) - \frac{\epsilon}{\sigma}\left(\tilde{\nabla}^2 - \frac{j^2}{r}\right) T_j^{c,s}$$

$$= -\left\{\frac{1}{r}\frac{\partial}{\partial r}(ru_j^{c,s} T_0) \pm \frac{j}{r}(v_0 T_j^{s,c} + v_j^{s,c} T_0) + \frac{\partial}{\partial z}(w_j^{c,s} T_0)\right\} + \mathcal{N}^{c,s}(T)_j, \quad (17a,b)$$

$$\frac{1}{r}\frac{\partial}{\partial r}(ru_j^{c,s}) \pm \frac{j}{r} v_j^{s,c} + \frac{\partial}{\partial z} w_j^{c,s} = 0. \quad (18a,b)$$

The boundary conditions are

$$u_j^{c,s} = v_j^{c,s} = w_j^{c,s} = 0 \qquad \text{at } r = A_2, 1 + A_2 \text{ and } z = 0$$

$$\frac{\partial}{\partial z} u_j^{c,s} = \frac{\partial}{\partial z} v_j^{c,s} = w_j^{c,s} = 0 \qquad \text{at } z = A_1,$$

$$T_j^{c,s} = 0 \qquad \text{at } r = A_2, 1 + A_2, \quad (19)$$

$$\frac{\partial}{\partial z} T_j^{c,s} = 0 \qquad \text{at } z = 0, A_1.$$

The terms $\mathcal{N}_j$ represent the nonlinear wave–wave interactions, which consist of components of wavenumbers n and m, such that $|m - n| = j$ for $1 \leqslant j, m, n \leqslant K$, and where K is the highest wavenumber included in the computation. Under two conditions, $\mathcal{N}_j$ may be set equal to zero: (a) when only one wavenumber is considered; (b) when more than one wavenumber is considered, but no sum or difference of any two of these wave numbers is equal to a third. The discussion below is primarily for case (a), although it automatically covers case (b)

The decomposition technique is standard and had been used previously in different context by Gilman [6].

4. Method of Solution

The mean field equations (9–13), and the amplitude equations (14)–(18) depend on r, z, and t. We have increased the number of unknowns to $(5 + 10J)$, where J is the number of azimuthal waves to be included, but have reduced the spatial dependence from three to two variables.

The equations are solved numerically by the finite difference method on variable grids. The momentum equations are solved semi-implicitly line by line in alternate directions (ADI) [22]. The temperature equations are solved as follows. The advective terms are represented by a variant of Roberts and Weiss' [19] angled derivatives and solved by fractional time steps. The diffusive terms are then solved

by ADI. Variable grids introduce variable coefficients into the pressure equations [see Eqs. (29b) and (30) below], which are elliptic, and the equations are solved by ADI with variable acceleration parameters. For each time step, the time dependent equations are interated once. The pressure equations are iterated four times.

In Section (a) variable grids through coordinate transformation are introduced. In Section (b) the net and the finite difference approximation to the differential equations are described; the finite difference equation for the zonally averaged pressure, p_0, is formulated explicitly. In Section (c) the computation procedure is given. The complete set of transformed equations and their finite difference representations are given in the Appendixes A and B.

(a) *Variable Grid through Coordinate Transformation*

Variable grids are introduced implicitly into the computational scheme through a change of coordinates in the equations. This method has been discussed by various authors [1, 9, 18, 20].

Consider the coordinate transformation from $r \to \xi(r)$, and $z \to \eta(z)$ in the equations. If ξ and η are not linear functions of r and z, a net of constant grid intervals in the ξ–η plane will correspond to variable grids in the r–z plane.

Following [18], we make the following transformation.

$$\xi(r) = \frac{(L+1)}{2} + \frac{(L-1)}{2} \cdot \frac{\ln\{(b_1 + x(r))/(b_1 - x(r))\}}{\ln\{(b_1 + a_1)/(b_1 - a_1)\}},$$

$$\eta(z) = \frac{(N+1)}{2} + \frac{(N-1)}{2} \cdot \frac{\ln\{(b_2 + y(z))/(b_2 - y(z))\}}{\ln\{(b_2 + a_2)/(b_2 - a_2)\}}, \qquad (20a, b)$$

where

$$x = r - (A_2 + \tfrac{1}{2}), \qquad y = z - (A_2/2),$$
$$a_1 = \tfrac{1}{2}, \qquad b_1^2 = a_1^2/(1 - d_1/a_1),$$
$$a_2 = A_1/2, \qquad b_2^2 = a_2^2/(1 - (d_2/a_2)).$$

L and N are the end points of ξ and η and are assigned integral values here, and

$$d_1 < a_1, \qquad d_2 < a_2.$$

When d_1 and d_2 approach zero, the grid points in the r, z plane become more compact near the boundaries. Figure 2 is a plot of ξ versus x with $d_1 = 0.15$, $L = 25$. Note that ξ takes on integral values from 1 to L. Roberts has explained in detail the advantage of the above choice of functions. The transformed equations are given in Appendix A.

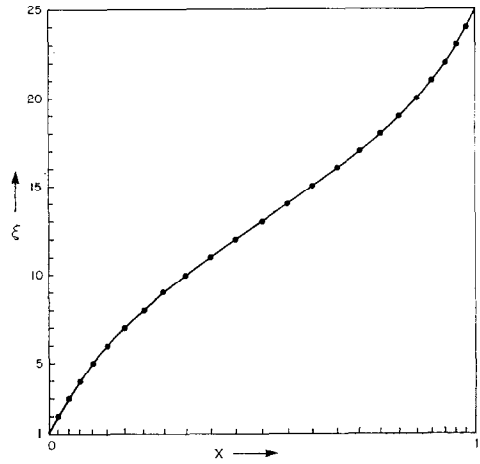

FIG. 2. Transformation of x into ξ. Note that integral numbers of ξ from 1 to 25 correspond to fractional values of x from 0 to 1, $d_1 = 0.15$. In the computation, $\Delta\xi = \Delta\eta = 1$.

(b) *The Net and Finite Difference Formulation*

The net is depicted in Fig. 3. The cross section of the annulus is divided into uniform square cells on the ξ–η plane. At the center of the cells the variables V, T, and P are defined. At the midpoints of the cell walls, the normal velocities are prescribed. Boundary surfaces of the annulus are placed along the cell boundaries. The net is extended a fraction of a grid distance beyond each physical boundary. As suggested by both Roberts [18] and Kalnay de Rivas [9], the outermost grid points are placed at the same distance from the physical boundaries as the first inner grid point within the boundary. The variables on the outermost grid points are determined from the second outermost points and the boundary conditions.

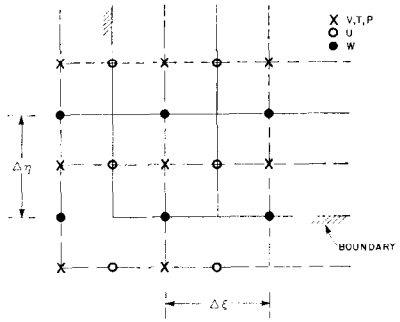

FIG. 3. Relative positions of the variables on staggered grids.

We shall represent time and space by $t = \nu\,\Delta t$, $\xi = i\,\Delta\xi$, and $\eta = k\,\Delta\eta$, where ν, i, and k are integers; $\Delta\xi = \Delta\eta = 1$ are spatial grid intervals: and Δt is the time step. For compactness, the following contracted notations are used.

$$\begin{aligned}
f(\xi, \eta; t) &= f(i\Delta\xi, k\Delta\eta; \nu\Delta t) = f_{ik}^{\nu}, \\
\delta_t{}^{+} f^{\nu+(1/2)} &= (f^{\nu+(1/2)} - f^{\nu})/(\Delta t/2), \\
\delta_t{}^{+} f^{\nu+1} &= (f^{\nu+1} - f^{\nu+(1/2)})/(\Delta t/2), \\
\delta_I f_{ik} &= (\delta_\xi f)_{ik} = (f_{i+(1/2),k} - f_{i-(1/2),k}), \\
\delta_k f_{ik} &= (\delta_\eta f)_{ik} = (f_{i,k+(1/2)} - f_{i,k-(1/2)}), \\
\bar{f}_{ik}^{I} &= (f_{i+(1/2),k} + f_{i-(1/2),k})/2, \; \bar{f}_{ik}^{K} = (f_{i,k+(1/2)} + f_{i,k-(1/2)})/2, \\
I_r &= \partial\xi/\partial r, \qquad K_z = \partial\eta/\partial z.
\end{aligned} \tag{21}$$

Only the mean pressure equation will be derived in detail here. The other equations are given in Appendix B.

We have, from Eqs. (A.11) and (A.13) in Appendix B,

$$\begin{aligned}
\delta_t{}^{+} u_0^{\nu+(1/2)} &= \epsilon K_z \delta_k (K_z \delta_k u_0)^{\nu+(1/2)} + \epsilon I_r \delta_I (I_r/r\ \delta_I r u_0)^{\nu} \\
&\quad - I_r \delta_I p_0^{\nu+(1/2)} + R u_0{}^{\nu} + 0(\Delta t),
\end{aligned} \tag{22a}$$

$$\begin{aligned}
\delta_t{}^{+} u_0^{\nu+1} &= \epsilon K_z \delta_k (K_z \delta_k u_0)^{\nu+(1/2)} + \epsilon I_r \delta_I (I_r/r \delta_I r u_0)^{\nu+1} \\
&\quad - I_r \delta_I p_0^{\nu+(1/2)} + R u_0{}^{\nu} + 0(\Delta t),
\end{aligned} \tag{22b}$$

$$\begin{aligned}
\delta_t{}^{+} w_0^{\nu+(1/2)} &= \epsilon K_z \delta_k (K_z \delta_k w_0)^{\nu} + \epsilon I_r \delta_I (r I_r \delta_I w_0)^{\nu+(1/2)} \\
&\quad - K_z \delta_k p_0^{\nu+(1/2)} + R w_0{}^{\nu} + 0(\Delta t),
\end{aligned} \tag{23a}$$

$$\begin{aligned}
\delta_t{}^{+} w_0^{\nu+1} &= \epsilon K_z \delta_k (K_z \delta_k w_0)^{\nu+1} + \epsilon I_r/r \delta_I (r I_r \delta_I w_0)^{\nu+(1/2)} \\
&\quad - K_z \delta_k p_0^{\nu+(1/2)} + R w_0{}^{\nu} + 0(\Delta t),
\end{aligned} \tag{23b}$$

$$I_r/r\ \delta_I (r u_0)^{\nu+1} + K_z \delta_k w_0^{\nu+1} = 0, \tag{24}$$

where Ru_0 and Rw_0 are contracted notations for the rest of the terms in Eqs. (A.11a, b) and (A.13a, b). The advective terms, which are formulated semi-implicitly in Eqs. (A.11) and (A.13), have been assumed to contain velocities at the νth, instead of the $(\nu + \frac{1}{2})$th time step. An error $O(\Delta t)$ has been thus introduced.

If we subtract (22b) from (22a), and (23b) from (23a), and rearrange terms, we have

$$\begin{aligned}
u_0^{\nu+(1/2)} &= \tfrac{1}{2}\,(u_0^{\nu+1} + u_0{}^{\nu}) \\
&\quad + (\epsilon\,\Delta t/4)\, I_r \delta_I (I_r/r \delta_I r \{u_0{}^{\nu} - u_0^{\nu+1}\} + 0(\Delta t^2),
\end{aligned} \tag{25}$$

$$w_0^{\nu+(1/2)} = \tfrac{1}{2}(w_0^{\nu+1} + w_0{}^{\nu}) + (\epsilon\,\Delta t/4)\,K_z\delta_k K_z\delta_k(w_0{}^{\nu} - w_0^{\nu+1}) + 0(\Delta t^2). \tag{26}$$

Now add (22a) to (22b) and (23a) to (23b):

$$(u_0^{\nu+1} - u_0{}^{\nu})/\Delta t = \epsilon K_z\delta_k K_z\delta_k u_0^{\nu+(1/2)} + \epsilon I_r\delta_I I_r/r\;\delta_I\{r(u_0^{\nu+1} + u_0{}^{\nu})/2\} - I_r\delta_I p_0^{\nu+(1/2)} + Ru_0{}^{\nu} + 0(\Delta t), \tag{27}$$

$$(w_0^{\nu+1} - w_0{}^{\nu})/\Delta t = \epsilon K_z\delta_k K_z\delta_k\{(w_0^{\nu+1} + w_0{}^{\nu})/2\} + \epsilon I_r/r\;\delta_I r I_r\delta_I w_0^{\nu+(1/2)} - K_z\delta_k p_0^{\nu+(1/2)} + Rw_0{}^{\nu} + 0(\Delta t). \tag{28}$$

To obtain an equation for $p_0^{\nu+(1/2)}$, substitute (25) and (26) into (27) and (28). Operate on (27) with $(I_r/r)\,\delta_I(r\cdot)$, on (28) with $K_z\delta_k$, and use the finite difference divergence and Laplacian operators

$$\nabla\cdot\mathbf{V}_0 = I_r/r\;\delta_I(ru_0) + K_z\delta_k w_0\,, \qquad \nabla^2 p_0 = I_r/r\;\delta_I r I_r\delta_I p_0 + K_z\delta_k K_z\delta_k p_0 \tag{29a,b}$$

to obtain

$$\nabla^2 p_0^{\nu+(1/2)} = I_r/r\;\delta_I(r\cdot Ru_0{}^{\nu}) + K_z\delta_k(Rw_0{}^{\nu}) + \left(\frac{1}{\Delta t} + \frac{\epsilon}{2}\nabla^2 + \frac{\epsilon^2\,\Delta t}{4} I_r/r\;\delta_I r I_r\delta_I K_z\delta_k K_z\right)\nabla\cdot\mathbf{V}_0{}^{\nu} - \left(\frac{1}{\Delta t} - \frac{\epsilon}{2}\nabla^2 + \frac{\epsilon^2\,\Delta t}{4} I_r/r\;\delta_I r I_r\delta_I K_z\delta_k K_z\right)\nabla\cdot\mathbf{V}_0^{\nu+1} + 0(\Delta t). \tag{30}$$

We use the accepted procedure [7] to force the unknown velocity in (30), $\mathbf{V}_0^{\nu+1}$, to satisfy the continuity equation $\nabla\cdot\mathbf{V}_0^{\nu+1} = 0$, but to retain $\nabla\cdot\mathbf{V}_0{}^{\nu} = \mathscr{D}_0{}^{\nu}$, which is nonzero but small. To be consistent with the approximation in the advective terms, we shall discard $O(\Delta t)$ terms in (30); thus,

$$\nabla^2 p_0^{\nu+(1/2)} = I_r/r\;\delta_I(rRu_0{}^{\nu}) + K_z\delta_k Rw_0{}^{\nu} + \left(1 + \frac{\epsilon\,\Delta t}{2}\nabla^2\right)(\mathscr{D}_0{}^{\nu}/\Delta t) + 0(\Delta t). \tag{30a}$$

We note that ∇^2 in (29b) has variable coefficients (I_r, K_z depend on the spatial coordinates). There are various ways to solve the elliptic equation (30a). For example Swarztrauber's [21] modified Buneman's elliptic solver is quite efficient. But ADI with variable acceleration parameters [22] is almost as efficient, and simpler. The pressure of the previous time step, $p_0^{\nu-(1/2)}$, is used as the initial value

to start the iterations. It has been found that four iterations of the ADI give sufficiently accurate results in the range of physical parameters we are interested in.

The boundary conditions for $p_0^{\nu+(1/2)}$ can be obtained from (27) and (28) as follows.

On the vertical walls $u = v = w = 0$ at all times, and (27) reduces to

$$\delta_I p_0^{\nu+(1/2)} = \epsilon \delta_I \{I_r/r\, \delta_I r u_0^{\nu}\} + 0(\Delta t). \tag{31}$$

Similarly, on the horizontal boundaries (28) reduces to

$$\delta_k p_0^{\nu+(1/2)} = \epsilon \delta_k \{K_z \delta_k w_0^{\nu}\} + \beta T_0^{\nu} + 0(\Delta t). \tag{32}$$

The second derivatives of the normal velocities on each boundary are required in (31) and (32). The calculation of these second derivatives requires the first derivatives. More explicitly, either $I_r/r\delta_I(ru)$, or $K_z\delta_k w$ is required immediately outside the boundaries. To obtain these undefined quantities outside the boundaries, we let the divergence at the grid points immediately outside the boundary assume some value D, i.e.,

$$(I_r/r)\, \delta_I(ru_0) + K_z \delta_k w_0 = D.$$

Outside the vertical boundaries, $K_z\delta_k w_0$ is known. If D is given, $I_r/r\delta_I(ru_0)$ can be computed from the above equation. Similarly, outside the horizontal boundaries, $I_r/r\delta_I(ru_0)$ is known. $K_z\delta_k w_0$ can be calculated. Again we follow [7] and set $D = 0$. Although other possibilities have been tried, e.g., the normal gradient $(\partial/\partial\eta)(\nabla \cdot \mathbf{V}_0) = 0$ or $\nabla \cdot \mathbf{V}_0 = 0$ on the boundaries, neither of these conditions affects the final result. The physical explanation is that the nonhydrostatic pressure in an annulus is largely determined by the shear of the zonal current and density stratification in the interior. They serve as sources of the potential, p, in Eq. (30a). When ϵ is sufficiently small, the two terms containing ϵ in (31) and (32) do not play a strong role in determining the solution of (30a), although they serve as part of the boundary conditions.

The equations for p_j^c and p_j^s can be formulated in a similar way (see Appendix B).

(c) *Procedure of Computation*

The following procedure of computation is recommended for problems containing one or more waves. First, integrate the mean field equations to some advanced state (not necessarily the steady state). Perturb the $T^{c,s}$ equations with a random field of almost arbitrary magnitude [perturbation $O(10^{-3})$ to $O(10^{-2})$

vs the maximum side wall temperature ± 0.5, have been used]. After integrating the whole set of equations a few rotations beyond the perturbation, finite amplitude waves should develop. This seems to be the most natural way to introduce a perturbation. Certainly it saves overall computing time. Williams [23] and Dietrich [2] also used similar procedure in their computations. The fully developed wave solutions of one set of parameters have also been used as the initial condition to obtain finite amplitude waves for a different set of parameters. Unless the final state for the new set of parameters will be close to the initial condition used, this procedure is not recommended because large-scale oscillation is bound to be set up which can persist for a very long time. In general, it is not too time consuming to advance the two-dimensional computation to a reasonably steady stage in comparison with the rest of the computation after perturbation.

5. Stability Properties of the Algorithm

The full set of equations as given in Appendix B is too complex to analyze for stability criteria. We can, however, make some heuristic statements on the stability properties of the algorithm, and verify their validity by numerical experiments.

Theoretically, the most serious limiting factor, namely the diffusive time scale, has been removed by treating the diffusive terms implicitly. The Courant–Friedrichs–Lewy condition for advection, i.e., $\Delta t \leqslant \Delta x/U$, remains one of the necessary conditions to observe, although in practice, u and w are too small in this problem to cause concern. It turns out that the time step is limited by the inertial waves whose period is of order half the rotational period of the annulus. A simple calculation gives this limit. Consider the following coupled equations on staggered grids:

$$u_k^{\nu+1} - u_k{}^{\nu} = \Delta t/2\,(v_k{}^{\nu} + v_{k+1}^{\nu}),$$

$$v_k^{\nu+1} - v_k{}^{\nu} = -\Delta t/2\,(u_{k-1}^{\nu+1} + u_k^{\nu+1}).$$

If the kth Fourier components $u_k{}^{\nu} = \xi^{\nu} e^{ik\Delta x}$, $v_k{}^{\nu} = \eta^{\nu} e^{ik\Delta x}$ are substituted into the above equations, the amplification matrix [17] is obtained:

$$G(\Delta t, k) = \begin{pmatrix} 1 & \alpha(1 + e^{i\Delta x}) \\ -\alpha(1 + e^{-i\Delta x}) & 1 - 2\alpha^2(1 + \cos \Delta x) \end{pmatrix}, \qquad \alpha = \Delta t/2.$$

The eigenvalues for $G(\Delta t, k)$ are

$$\lambda_{\pm} = 1 - (\alpha^2\gamma^2 \pm \alpha\gamma(\alpha^2\gamma^2 - 4)^{1/2})/2,$$

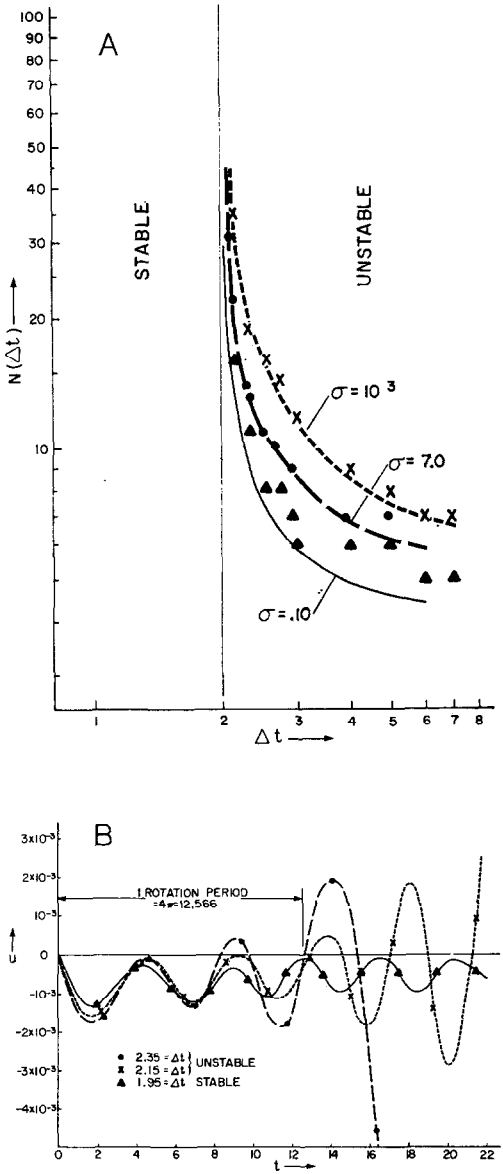

FIG. 4. (A) Stability curves for numerical experiments of three different values of σ. All other parameters are the same as Williams' case given in Section 7. (B) Amplification and decay of inertial waves, depending on whether Δt is larger or less than 2.0. The data points are from consecutive time steps.

where

$$\gamma^2 = 2(1 + \cos \Delta x) \leqslant 4.$$

For computational stability we require $\lambda\lambda^* \leqslant 1$, or $0 \leqslant \alpha \leqslant 1$, which is equivalent to $0 \leqslant \Delta t \leqslant 2$. Thus, Δt has to be equal to or less than, 2.

The results of a series of numerical experiments are given in Fig. 4A. The graphs show the number of cycles $N(\Delta t)$, for which the computation "blew up" as a function of the time steps Δt. The upper limit for computational stability is unmistakably at $\Delta t = 2.0$, as predicted. Note that for all three values of σ, the computations as shown in Fig. 4A are stable up to 100 time steps at $\Delta t = 2.0$. No experiments were carried out beyond 100 time steps.

To show that inertial waves are indeed responsible for the instability, we have plotted in Fig. 4B the radial velocity u as a function of time at a point $I = 24$, $k = 24$ in a 26×26 grid, that is, a point at the upper right-hand corner next to the hot wall. The three curves correspond to three values of $\Delta t = 1.95$, 2.15, and 2.35. Only the first few cycles of the computation are plotted, but this is adequate to demonstrate the effect of various values of Δt. It is clear that waves of comparable amplitude and period are initially excited in all three cases. The periods are all of order 2π, half the rotational period. In the two cases where Δt is larger than 2.0, these waves grew very rapidly without bound, while in the case with $\Delta t = 1.95$, the wave decayed slowly. In the computation that yielded the results discussed below, Δt was taken to be 1.40 for the two-dimensional computation (mean field equations only) and 0.90 for the three-dimensional computation. At the time of the computation, it was necessary to choose the Δt values prudently because there was very little experience on how the whole system would behave in a long computation.

6. Scope of Numerical Experiments

Four separate numerical experiments with one wavenumber were carried out. The first three experiments were exploratory in nature. They were done on exceedingly coarse, and nearly constant, grids but they have helped to establish the computational procedures. Although the results of these three computations are not sufficiently accurate to give details of the flows they exhibit all the characteristics of baroclinic waves. The energetics compare very well with those found by Pfeffer *et al.* [15] in the laboratory.

The fourth case is a repeat of Williams' computation. The purpose is to ensure that the present algorithm produces the main feature, if not all, of Williams' three-dimensional results.

In the next section, we shall examine the results of this particular case in detail.

7. Comparison of Numerical Results

Williams has already described the three-dimensional structure of steady annulus waves. It is not the intention to repeat these analyses here but only to show that the present model can reproduce all the main results generated by Williams' three-dimensional finite difference scheme. Thus, the following important question concerning the present model is answered in the affirmative. Can one wavenumber adequately represent at least the most simple three-dimensional flow, i.e., a steady traveling wave?

The set of nondimensional numbers used for the computation is $\beta = 0.13125$, $\epsilon = 6.9997 \times 10^{-4}$, $\sigma = 7.0986$, $A_1 = 1$, $A_2 = \frac{2}{3}$, $Ra = \sigma\beta\epsilon^{-2} = 1.90 \times 10^6$, which are very close to Williams' parameters. The coordinate stretching parameters are $d_1 = d_2 = 0.15$. The net consists of 26×26 grid points. If we take $\epsilon^{1/2} = 2.65 \times 10^{-2}$, $Ra^{-1/4} = 2.69 \times 10^{-2}$ as the order of magnitude of the horizontal and vertical boundary layer thicknesses, we have about two grid points within the maximum of each boundary layer. The total number of grid points may seem very moderate, but it is equivalent to the number of points that a net of 50×50 constant grids can provide to the boundary layers. Hence, the resolution in the boundary region should be comparable to the 32×32 constant grids used by Williams. Figure 5 shows plots of (A) the vertical velocity and temperature at $z = 0.62$ near the cold wall, and (B) the Ekman boundary-layer velocities off the lower boundary. The plots show the distribution of grid points in the boundary layers. We note that the "eddy" fields (indicated by superscripts c and s) are comparable in magnitude with the zonally averaged fields (subscripted 0). This clearly shows that the waves are of finite amplitude. The linearized theories of baroclinic instability, which assume infinitesimal waves, may not be able to explain all the computed results.

To compare Williams' results, the velocity fields must be multiplied with the characteristic $U = 2\Omega L = 4.80$ cm/sec, and the stream function with $\psi = 2\Omega L^3 = 43.2$ cm^3/sec. It is not as straightforward to compare the pressure fields, as will be explained later.

a. *The Axisymmetric Fields*

The axisymmetric fields are computed from the complete two-dimensional Navier–Stokes equations and the heat equation, i.e., Eqs. (9)–(13), with the self-interaction terms containing u_i^c, u_j^s, etc., deleted. The question of whether one wavenumer in the third dimension is adequate or not is not involved in a two-dimensional computation. Consequently, any differences we may find between Williams' and our results can be totally attributed to the difference in the numerical approximation.

Figures 6a–6f show the stream function ψ, normalized temperature T, zonal

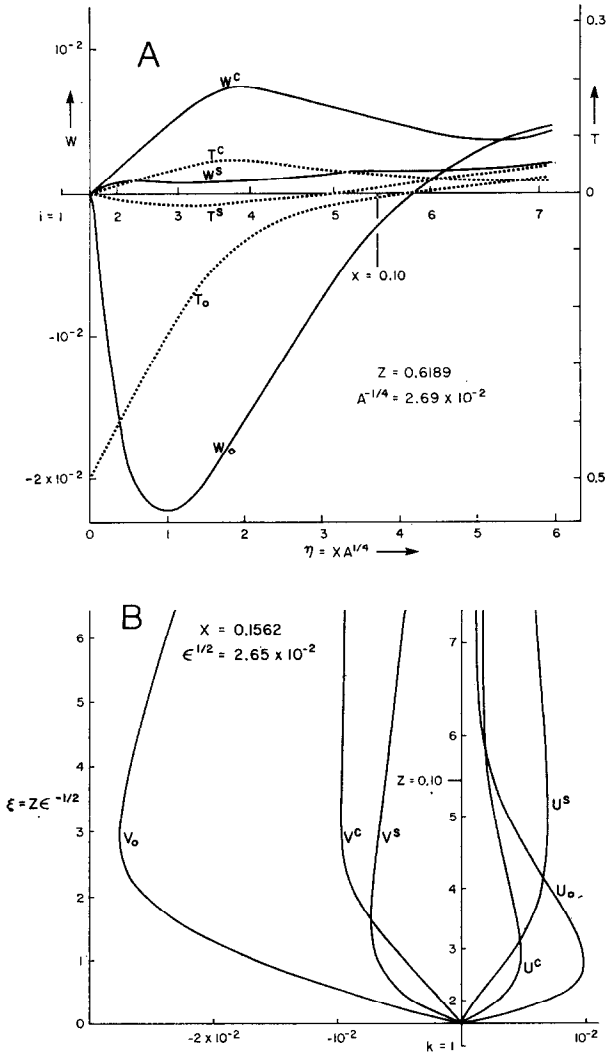

FIG. 5. (A) Vertical velocity and temperature components in the vertical boundary layer near the cold wall are plotted as functions of the stretched coordinate $\eta = xA^{1/4}$, A being the Rayleigh number, and as functions of the variable grids $i = 1, 2,...$ superimposed on the x axis, the radial distance from the inner wall of the annulus. Note that the range of x is $0 \leqslant x \leqslant 1$. The boundary layer is about 1/10 the width of the annulus. There are about five grid points in the layer. (B) Horizontal velocity components u and v in the lower Ekman layer in the inner sector of the annulus are plotted as functions of the vertical stretched coordinate $\xi = z\epsilon^{-1/2}$and also as function of the variable grids, $k = 1, 2,....$ There are about five grid points in the Ekman layer.

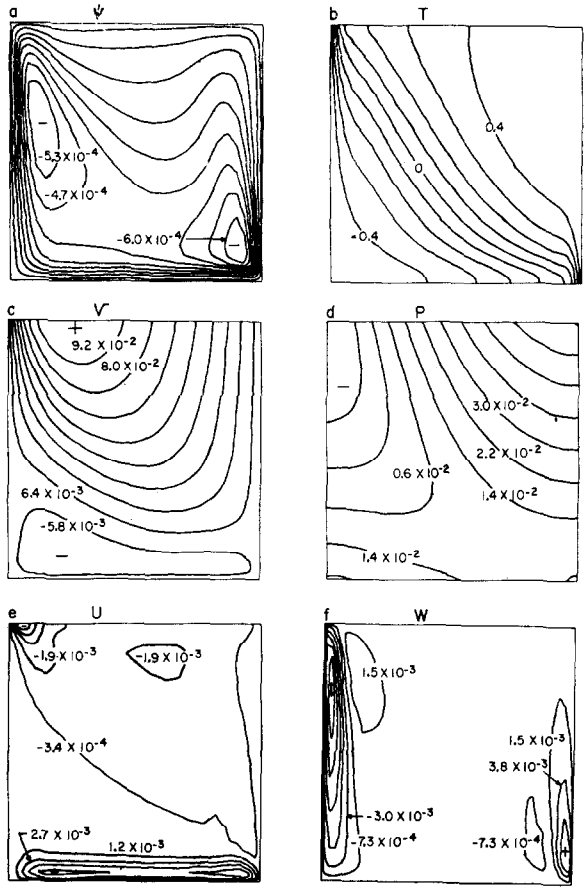

FIG. 6. Contour plots of field variables for the two-dimensional (axisymmetric) computation. The maxima and minima of each field are given. Contour intervals are (Max–Min)/10 for each field. At least one contour line is identified in each diagram. $\psi_{max} = 0.0$, $\psi_{min} = -6.70 \times 10^{-4}$; $T_{max} = 0.50$, $T_{min} = -0.50$; $V_{max} = 1.04 \times 10^{-1}$, $V_{min} = -1.80 \times 10^{-2}$; $P_{max} = 6.14 \times 10^{-2}$, $P_{min} = -1.70 \times 10^{-2}$; $U_{max} = 7.38 \times 10^{-3}$, $U_{min} = -8.07 \times 10^{-3}$; $W_{max} = 8.38 \times 10^{-3}$, $W_{min} = -1.44 \times 10^{-2}$.

velocity v, and dynamic pressure p; and the radial and vertical velocities, u and w.

The first four diagrams are arranged in the same order as Williams' [4, Fig. 4a] for easy comparison. Except for the obvious differences in the pressure field, which we shall discuss later, the qualitative agreement in the shapes of the stream lines, isotherms, and isotachs for the zonal velocity is good.

Perhaps the most meaningful quantity to compare with that of Williams is the

zonal velocity. The nondimensional maximum is 0.104 (which is also the Rossby number) and the minimum is -0.018, which correspond to 0.501 and -0.085 cm/sec as compared to Williams' values of 0.52 and -0.08 cm/sec, respectively.

The stream function is obtained from the simple formula

$$\psi_{ik} = -\sum_{l=1}^{k} r_l/(K_z)_l \, u(i, l).$$

In Fig. 6a, the nondimensional absolute maximum (lower right-hand corner) is 6.70×10^{-4} or 2.89×10^{-2} cm^3/sec as compared to (approximately) 3.0×10^{-2} cm^3/sec in Williams' computation. The three stream lines of the lower right-hand cell are, in ascending order, -2.59×10^{-2}, -2.29×10^{-2}, and -1.99×10^{-2} cm^3/sec vs Williams' corresponding stream lines of -2.5×10^{-2}, -2.3×10^{-2}, and -2.0×10^{-2} cm^3/sec. It appears that Williams' lower cell goes as high as -3.5×10^{-2} cm^3/sec, though only a very small area would assume this value. The outer two stream lines compare well with those of Williams in the upper left-hand cell, but the innermost stream line in Williams' diagrams cover a larger area. In spite of these differences the general shape and curvature of both stream functions agree remarkably well. The numerical values of the corresponding isotherms are the same when scaled by a proper factor. The comparison one should make in the temperature field is the position of the isotherms. Most of the results of the two computations are virtually identical.

The difference in the pressure field is due to the different ways the temperatures are defined in the respective computations. The normalized temperature used in the present model is defined as

$$T^* = (T - \overline{T})/\Delta T, \qquad \overline{T} = (T_0 + T_1)/2, \qquad \Delta T = (T_1 - T_0)$$

and Williams' dimensional temperature is normalized as

$$\tilde{T} = (T - T_0) = (T - \overline{T}) - (\overline{T} - T_1).$$

If we nondimensionalize $\tilde{T}$ with ΔT, we have

$$\tilde{T}^* = \tilde{T}/\Delta T = T^* + (T_1 - \overline{T})/\Delta T = T^* + \text{positive constant},$$

since $T_1 > \overline{T}$.

For geostrophic flow, the isobaric slope is given by

$$(\partial p/\partial r/\partial p/\partial z)_{p=\text{const}} = -v/(\beta T^*)$$

for the present computation, and for Williams, it is

$$(\partial p/\partial r/\partial p/\partial z)_{p=\text{const}} = -v/\beta(T^* + \text{const}).$$

Therefore, in the interior where the dynamics are essentially geostrophic the magnitude of our isobaric slopes ought to be larger than those of Williams. In comparison with our pressure field, Williams has an additional component linear in z, which is essentially hydrostatic.

Radial and vertical velocities are contoured in Figs. 6e and 6f. If we take the outer contour lines of the velocities as the outer edges of the respective boundary layers, we have about five grid points across the layers at midpoint (also see Fig. 5).

b. *The Wave Fields*

(i) *The zonally averaged (mean) fields.* The zonally averaged fields of the wavenumber 5 computation are depicted in Fig. 7. They are to be compared with Williams' [24, Figs. 4b]. A visual comparison shows that the mean fields appear similar, except that (1) Williams' maximum zonal current near the surface of the fluid is much closer to the inner wall, and (2) upper isotherms of the present computation shown in Fig. 7b are more detached from the boundary region in the upper left-hand corner.

A quantitative comparison of ψ_0 and v_0 is now given. ψ_0 is calculated from u_0 by $(\psi_0)_{ik} = -\sum_{l=1}^{k} r_i/(K_z)_l \, u_0(i, l)$.

The maximum and minimum of ψ_0 are 3.80×10^{-4} and -10.4×10^{-4}, or 1.64×10^{-2} cm^3/sec, and -4.49×10^{-2} cm^3/sec, respectively. There are nine contour lines between the maximum at the center of the middle cell and the minima at the centers of the side cells (the absolute value of the right-hand one is slightly larger). The contour interval is $(1.64 + 4.49) \times 10^{-3} = 6.13 \times 10^{-3}$ cm^3/sec. While the general positions of the streamlines seem to agree well with Williams' [24, Fig. 4bi], in which the minimum in the lower right-hand cell is less than -5.0×10^{-2} cm^3/sec, compared to -4.49×10^{-2} cm^3/sec in Fig. 7a, there is a difference of about 9 %.

The maximum nondimensional zonal velocity, as shown in Fig. 7c, is 7.365×10^{-2} or 3.535×10^{-1} cm/sec vs Williams' maximum of 3.0×10^{-1} cm/sec. The minimum inside the lower left-hand corner [illegible]

These comparisons do show differences in the absolute maxima and minima of both the meridional and zonal flows, despite the similarity in the general circulation. In evaluating these differences, we must also bear in mind that we are comparing two different avarages. To see the difference, we represent any of our fields by

$$f(r, \phi, z; t) = f_0(r, z; t) + f'(r, \phi, z; t),$$

and our mean fields are

$$\bar{f}(r, \phi, z; t) = f_0(r, z; t) + (1/2\pi) \int_0^{2\pi} f'(r, \phi, z; t) \, dq = f_0(r, z; t).$$

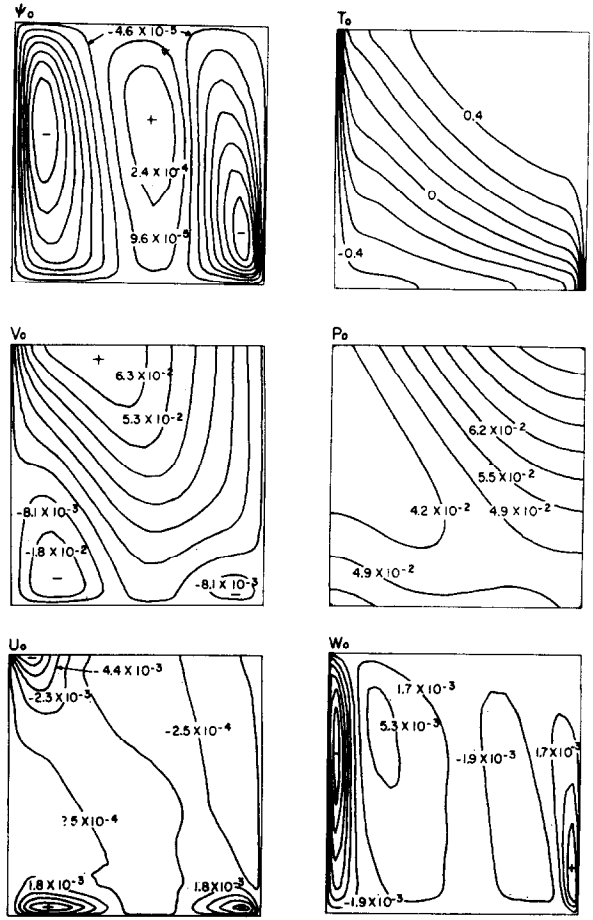

FIG. 7. Contour plots of zonal averaged field. (See caption of Fig. 6 for details). $(\psi_0)_{\max} = 3.80 \times 10^{-4}$, $(\psi_0)_{\min} = -1.04 \times 10^{-3}$; $(T_0)_{\max} = 0.50$, $(T_0)_{\min} = -0.50$; $(V_0)_{\max} = 7.36 \times 10^{-2}$, $(V_0)_{\min} = -2.85 \times 10^{-2}$; $(P_0)_{\max} = 9.38 \times 10^{-2}$, $(P_0)_{\min} = 2.95 \times 10^{-2}$; $(U_0)_{\max} = 1.00 \times 10^{-2}$ $(U_0)_{\min} = -1.05 \times 10^{-2}$; $(W_0)_{\max} = 1.25 \times 10^{-2}$, $(W_0)_{\min} = -2.35 \times 10^{-2}$.

We assume the integral of f' to be zero from the start. However, Williams' results are

$$\bar{f}(r, z; t) = f_0(r, z; t) \cdot (1/\Phi) \sum_{i=1}^{N} \Delta\phi_i + (1/\Phi) \sum_{i=1}^{N} f'(r, \phi, z; t)\, \Delta\phi_i .$$

Even if f' is truly sinusoidal, the last summation is not equal to zero because of truncation error. Differences in the averaged fields may be due to the different

averaging processes we used. Therefore, for a complex system like the present one, it is very difficult to assess the absolute accuracy of the results.

Figures 7e and 7f show contours of the zonally averaged radial and vertical velocities. The most obvious difference between the axisymmetric and the mean flow appears in the meridional circulation, which has become a three-cell system. The bottom Ekman layer in the axisymmetric flow has been broken into two parts, each being associated with the two side cells. The dynamics of a similar three-cell formation have been examined in terms of its energetics [15].

(ii) *The Fourier amplitudes.* The Fourier amplitudes of the wavenumber 5 computation are given in Figs. 8a–8j. Note that all Fourier amplitudes are time dependent. To have a complete picture of the cross-sectional structure, we must synthesize the total fields by Eqs. (7) and (8) for $0 \leqslant \phi \leqslant 2\pi/5$. Such a complete synthesis is not warranted here. We can, however, consider the cosine and sine components as the *complete* eddy components at different phases of the wave; e.g., at $5\phi = 0$ and $\pi/2$. The structures of the wave are very different at each phase. Since quasi-geostrophic balance holds in the interior at all times, from Eqs. (14) and (15) we have the balance

$$-(\partial/\partial r)\, p_j^{c,s} \simeq v_j^{c,s}, \qquad \pm(j/r)\, p_j^{s,c} \simeq -u_j^{c,s}.$$

The first expression shows that the radial pressure gradient $(\partial/\partial r)\, p_j{}^c(\, p_j{}^s)$ should balance the zonal velocity $v_j{}^s(v_j{}^s)$, and the second expression shows that the contours of $p_j{}^s(\, p_j{}^c)$ should be similar to those of $u_j{}^c(u_j{}^s)$. The contours in Figs. 8b, 8c, and 8i and 8a, 8d, and 8j show these balances in the region away from the bottom boundary. The vertical velocity $w_j^{c,s}$, pressure $p_j^{c,s}$, and temperature $T_j^{c,s}$ are studied in the subsection below.

Another noteworthy characteristic of the Fourier amplitudes is the obvious lack of dominant side boundary-layer structures, which are strong features of the mean field.

(iii) *Vertical and horizontal phase shifts.* Some of the most prominent features of baroclinic waves are the phase shift with height in the pressure field, the horizontal phase shift of vertical velocity from pressure, and the positive correlation of vertical velocity and temperature. These relations were originally given by Eady [3] as results of a linearized inviscid theory of baroclinic instability. In general, our results do show all these characteristics of baroclinic waves. In Figs. 9a–9i, the plan views of P, T, and W (the total sythesized fields) at three levels of z, 0.04, 0.59, and 0.94, are given. One can readily observe that:

(1) In spite of the distortion by the Ekman boundary layer at the bottom of the annulus, we can see, by comparing Fig. 9a with 9b, that there is a negative phase shift of about one-fourth wavelength in the pressure field from midlevel,

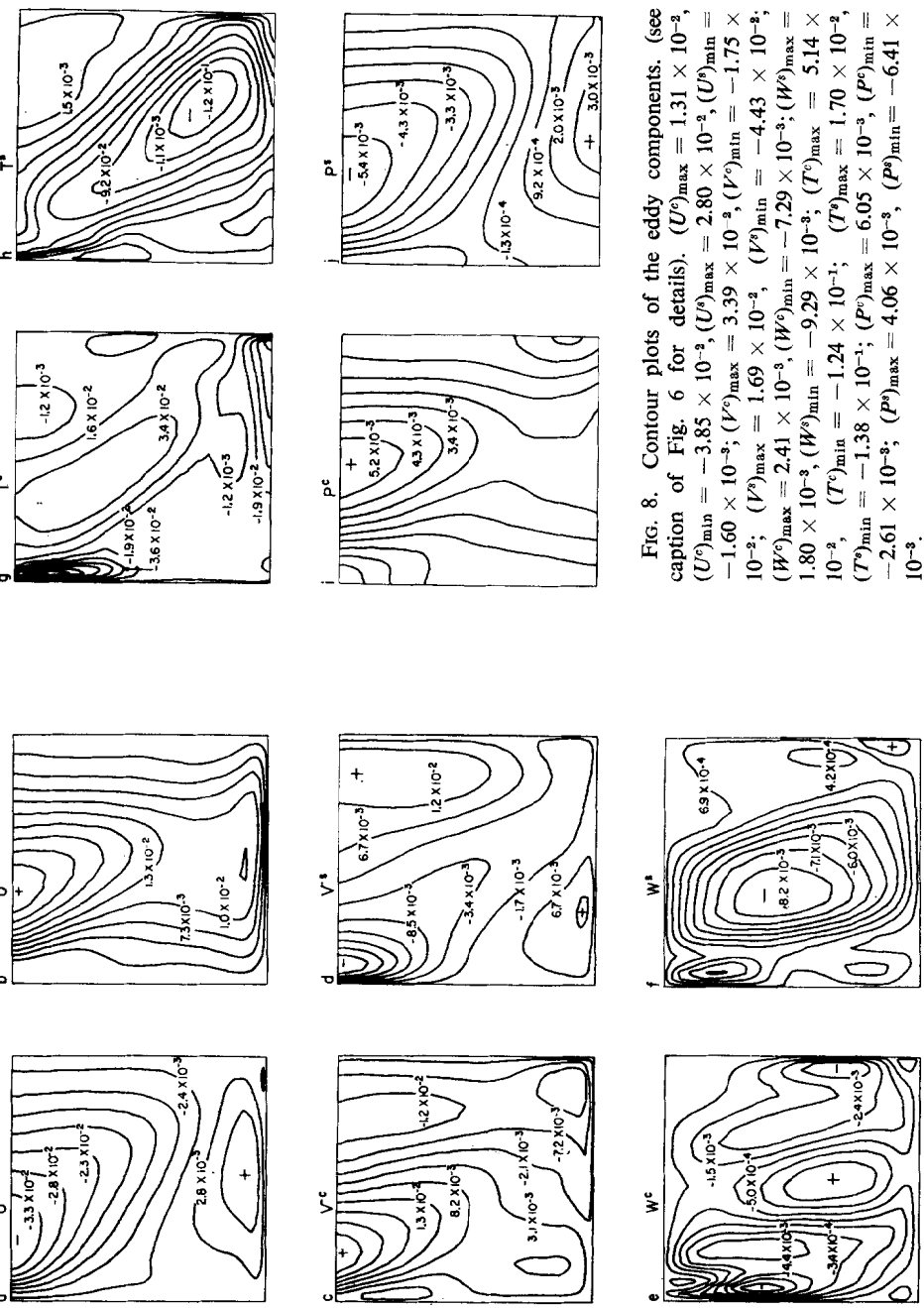

FIG. 8. Contour plots of the eddy components. (see caption of Fig. 6 for details). $(U^c)_{\max} = 1.31 \times 10^{-2}$, $(U^c)_{\min} = -3.85 \times 10^{-2}$, $(U^s)_{\max} = 2.80 \times 10^{-2}$, $(U^s)_{\min} = -1.60 \times 10^{-3}$; $(V^c)_{\max} = 3.39 \times 10^{-2}$, $(V^c)_{\min} = -1.75 \times 10^{-2}$; $(V^s)_{\max} = 1.69 \times 10^{-2}$, $(V^s)_{\min} = -4.43 \times 10^{-2}$; $(W^c)_{\max} = 2.41 \times 10^{-3}$, $(W^c)_{\min} = -7.29 \times 10^{-3}$; $(W^s)_{\max} = 1.80 \times 10^{-3}$, $(W^s)_{\min} = -9.29 \times 10^{-3}$, $(T^c)_{\max} = 5.14 \times 10^{-2}$, $(T^c)_{\min} = -1.24 \times 10^{-1}$; $(T^s)_{\max} = 1.70 \times 10^{-2}$, $(T^s)_{\min} = -1.38 \times 10^{-1}$; $(P^c)_{\max} = 6.05 \times 10^{-3}$, $(P^c)_{\min} = -2.61 \times 10^{-3}$; $(P^s)_{\max} = 4.06 \times 10^{-3}$, $(P^s)_{\min} = -6.41 \times 10^{-3}$.

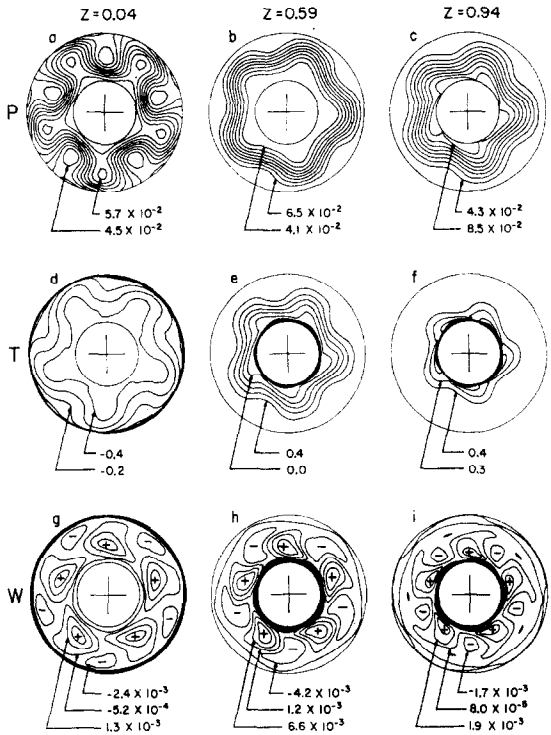

FIG. 9. The contours of the total pressure, temperature, and vertical velocity in the r–ϕ plane at three levels: $z = 0.04$, 0.59, and 0.94. Because of the crowding of many contour lines, two contour lines in each diagram are given. The contour intervals can be determined by the number of spacing between them. These three-dimensional fields are a synthesis of the field given in Figs. 7 and 8 from Eqs. (7) and (8b).

and that by comparing 9b and 9c the change from to midlevel the top is only barely perceptible. Williams [24] also showed similar relations. Eady's linearized theory for a fluid with a rigid lid predicts a negative shift of one-fourth wavelength from bottom to top of the fluid in P.

(2) If we compare T, Figs. 9d–9f, and W, Figs. 9g–9i, at the respective levels, there is a definite correlation between upwelling and high temperature, and downwelling and low temperature. This overturning in the zonal direction is the essential mechanism for conversion from eddy available potential energy to eddy kinetic energy in a baroclinic system. Pfeffer [15] observed that warm fluid rises ahead of the trough (low pressure) and cold fluid sinks behind it in the laboratory experiment as originally predicted by Eady [3]. This relationship also holds for the present results, as seen by comparing T and W at midlevel.

(3) It has already been pointed out that corss-sectional contours of the pressure fields in Figs. 7d, 8i, and 8j are very different from those of Williams. The isobaric contours in the r–ϕ plane are, however, similar to his, because at a given z-level the difference is a constant and hence will not show up in the r–ϕ contour.

(iv) *Wave Drift*

The drift speed of the waves is about $\Omega/30$ compared with $\Omega/24$ found by Williams. This discrepancy remains unexplained at present, although it is well known that different finite difference approximation in time and space can introduce [illegible] will show the relative accuracy of the computations.

8. Assessment of the Algorithm

For 26×26 grid points, the mean field equations take about 5 sec, and the full set of equations takes about 17 sec per time step on a CDC 6500. The Poisson and Helmholtz (pressure) equations consume about 25–30% of the total time. The nondimensional time step used for the computation of Williams' case is 0.90, approximately 1/14 of a rotational period, whereas Williams used a time step of about 1/157 of a rotational period.

For point-by-point computation, the present algorithm is naturally much slower than Williams' algorithm for two reasons: (a) The equations are more complicated because of the variable grids. (b) The present scheme is semi-implicit. The variable at each grid point is calculated twice consecutively for each time step (in the horizontal and the vertical directions).

There is a reduction in a computer storage requirement. Extending the computation from two to three space dimensions, we require 10 fields for each additional wavenumber, while a fully three-dimensional two-time level finite difference scheme would require $10 \times N$ fields, where N is the additional number of grid levels in the ϕ direction. To study the structure of one single baroclinic wave, one needs only to have N large enough to cover one wavelength as Williams has done (Williams used $N = 35$ for wavenumber 5). To represent two or more waves adequately with a fully three-dimensional finite difference scheme, one must have enough grid levels in the ϕ direction to cover the whole angular distance 2π instead of only one wavelegnth. Theoretically, with the amount of storage Williams used to calculate one single wave, we can accommodate 35 waves. But the computing time required for a 35-wave computation will be phenomenal, although the transformed method devised by Orszag [13, 14], Eliasen, Machenhauer, and Rasmussen [4], and Machenhauer and Rasmussen [11] will

no doubt be efficient methods to use when a large number of spectral components are included.

The total amount of computer time needed to obtain the results shown above for Williams' case was about 7 hr on CDC 6500, which is much less than the approximately 150 hr Williams used on a Univac 1108.

When only one wavenumber is used in the computation, all the higher harmonics are excluded, whereas they are automatically included in Williams' computation. As the laboratory experiments have shown, higher harmonics contain very little energy in simple annulus waves [15]. They certainly become more significant in complicated flows. This study has shown that for the case studied here the contribution from the higher harmonics is very small. Williams' finite difference algorithm has the distinct ability to start a computation without assuming what wave-number will dominate, while the present algorithm requires some prior knowledge. Considering the vast amount of available data on annulus waves, this deficiency is not a great handicap. The strength of the present model lies in its capability to simulate a single or a small number of three-dimensional baroclinic waves efficiently in a simple container.

9. Concluding Remarks

The mixed spectral and finite difference model presented here can, with one wavenumber, reproduce the major results achieved by Williams [23, 24]. It requires considerably less computer time and storage than previous models.

The model offers the possibility of efficiently studying problems such as:

(1) Location in parameter space of wave vacillation, wave dispersion, and similar phenomena. This is usually a time-consuming procedure.

(2) Interactions in baroclinic flows between mean current and wave, between wave and wave, or between multiple waves. This model simplifies these studies because it permits the selection of numbers of waves and wavenumbers.

(3) The energetic processes associated with different waves and their characteristics.

(4) Energy cascade in geostrophic turbulence among selected wavenumbers.

(5) Parameterization of baroclinic instability. A definitive solution of any of the first three problems will provide the basis for experiments in the parametrization of baroclinic instability.

We have only begun to delineate the nonlinear dynamics of some of these rather intricate processes in rotating and stratified fluids. The present algorithm will have much to contribute in future investigations.

APPENDIX A: THE TRANSFORMED EQUATIONS

If we transform the coordinates from $r \to \xi(r)$, $z \to \eta(z)$, we transform the differential operators as follows.

$$\left(\frac{\partial}{\partial r}, \frac{\partial}{\partial z}\right) \to \left(\xi_r \frac{\partial}{\partial \xi}, \eta_z \frac{\partial}{\partial \eta}\right),$$

$$\left(\frac{\partial}{\partial r} f(r) \frac{\partial}{\partial r}, \frac{\partial}{\partial z} g(z) \frac{\partial}{\partial z}\right) \to \left(\xi_r \frac{\partial}{\partial \xi} f(r(\xi))\, \xi_r \frac{\partial}{\partial \xi}, \eta_z \frac{\partial}{\partial \eta} g(z(\eta))\, \eta_z \frac{\partial}{\partial \eta}\right),$$

where $\xi_r = \partial\xi/\partial r$, $\eta_z = \partial\eta/\partial z$.
Equations (9)–(18) become the following, with the diffusive terms in (9) and (10) rewritten slightly differently:

$$\begin{aligned}\frac{\partial u_0}{\partial t} &+ \xi_r/r \frac{\partial}{\partial \xi}(r \cdot u_0^2) + \eta_z \frac{\partial}{\partial \eta}(w_0 u_0) - \epsilon\left(\xi_r \frac{\partial}{\partial \xi} \xi_r/r \frac{\partial}{\partial \xi} \cdot r + \eta_z \frac{\partial}{\partial \eta} \cdot \eta_z \frac{\partial}{\partial \eta}\right) u_0 \\ &= -\xi_r \frac{\partial}{\partial \xi} p_0 + \left(1 + \frac{v_0}{r}\right) v_0 - \xi_r/r \cdot \sum_l \frac{\partial}{\partial \xi} \cdot r \cdot (u_l^{c2} + u_l^{s2}) \\ &\quad - \eta_z \cdot \sum_l \frac{\partial}{\partial \eta}(u_l^c w_l^c + u_l^s w_l^s) + \frac{1}{r} \sum_l (v_l^{c2} + v_l^{s2}),\end{aligned} \tag{A.1}$$

$$\begin{aligned}\frac{\partial v_0}{\partial t} &+ \xi_r/r \frac{\partial}{\partial \xi}(r \cdot u_0 v_0) + \eta_z \frac{\partial}{\partial \eta}(w_0 v_0) - \epsilon\left(\xi_r \frac{\partial}{\partial \xi} \xi_r/r \frac{\partial}{\partial \xi} \cdot r + \eta_z \frac{\partial}{\partial \eta} \eta_z \frac{\partial}{\partial \eta}\right) v_0 \\ &= -\left(1 + \frac{v_0}{r}\right) u_0 - \xi_r/r \sum_l \frac{\partial}{\partial \xi} \cdot r \cdot (u_l^c v_l^c + u_l^s v_l^s) \\ &\quad - \eta_z \sum_l \frac{\partial}{\partial \eta}(w_l^c v_l^c + w_l^s v_l^s) - \frac{1}{r} \sum_l (u_l^c v_l^c + u_l^s v_l^s),\end{aligned} \tag{A.2}$$

$$\begin{aligned}\frac{\partial w_0}{\partial t} &+ \xi_r/r \frac{\partial}{\partial \xi}(r \cdot u_0 w_0) + \eta_z \frac{\partial}{\partial \eta} w_0^2 - \epsilon\left(\xi_r/r \frac{\partial}{\partial \xi} r \cdot \xi_r \frac{\partial}{\partial \xi} + \eta_z \frac{\partial}{\partial \eta} \eta_z \frac{\partial}{\partial \eta}\right) w_0 \\ &= -\eta_z \frac{\partial}{\partial \eta} p_0 + \beta T_0 - \xi_r/r \sum_l \frac{\partial}{\partial \xi} \cdot r \cdot (u_l^c w_l^c + u_l^s w_l^s) \\ &\quad - \eta_z \sum_l \frac{\partial}{\partial \eta}(w_l^{c2} + w_l^{s2}),\end{aligned} \tag{A.3}$$

$$\begin{aligned}\frac{\partial T_0}{\partial t} &+ \xi_r/r \frac{\partial}{\partial \xi}(r \cdot u_0 T_0) + \eta_z \frac{\partial}{\partial \eta}(W_0 T_0) - \epsilon/\sigma\left(\xi_r/r \frac{\partial}{\partial \xi} r \cdot \xi_r \frac{\partial}{\partial \xi} + \eta_z \frac{\partial}{\partial \eta} \eta_z \frac{\partial}{\partial \eta}\right) T_0 \\ &= -\xi_r/r \sum_l \frac{\partial}{\partial \xi} r \cdot (u_l^c T_l^c + u_l^s T_l^s) - \eta_z \sum_l \frac{\partial}{\partial \eta}(W_l^c T_l^c + W_l^s T_l^s),\end{aligned} \tag{A.4}$$

$$r^{-1} \xi_r \frac{\partial}{\partial \xi}(r \cdot u_0) + \eta_z \frac{\partial}{\partial \eta} w_0 = 0. \tag{A.5}$$

The following equations correspond to Eqs. (14)–(18) in Section 3; j is the wavenumber and hence an integer, and the following equations are called the jth component of the amplitude equations.

$$\begin{aligned}
&\frac{\partial}{\partial t} u_j^{c,s} + \xi_r/r \frac{\partial}{\partial \xi}(r \cdot u_0 \cdot u_j^{c,s}) + \eta_z \frac{\partial}{\partial \eta}(w_0 u_j^{c,s}) \\
&\quad - \epsilon \left(\xi_r \frac{\partial}{\partial \xi} \xi_r/r \frac{\partial}{\partial \xi} \cdot r - \frac{j^2}{r^2} + \eta_z \frac{\partial}{\partial \eta} \eta_z \frac{\partial}{\partial \eta} \right) u_j^{c,s} \\
&= - \xi_r \frac{\partial}{\partial \xi} p_j^{c,s} + \left(1 + \frac{2v_0}{r}\right) v_j^{c,s} \pm \epsilon \left(\frac{2j}{r^2}\right) v_j^{s,c} \\
&\quad - \left(\xi_r/r \frac{\partial}{\partial \xi}(r u_0 u_j^{c,s}) \pm \frac{j}{r}(v_0 u_j^{s,c} + u_0 v_j^{s,c}) \right. \\
&\quad \left. + \eta_z \frac{\partial}{\partial \eta}(u_0 w_j^{c,s}) \right) + \mathcal{N}^{c,s}(u)_j \,, \qquad \text{(A.6a,b)}
\end{aligned}$$

$$\begin{aligned}
&\frac{\partial}{\partial t} v_j^{c,s} + \xi_r/r \frac{\partial}{\partial \xi}(r u_0 v_j^{c,s}) + \eta_z \frac{\partial}{\partial \eta}(w_0 v_j^{c,s}) \\
&\quad - \epsilon \left(\xi_r \frac{\partial}{\partial \xi} r \xi_r \frac{\partial}{\partial \xi} \cdot \frac{1}{r} + 2\xi_r \frac{\partial}{\partial \xi} \cdot \frac{1}{r} - \frac{j^2}{r^2} + \eta_z \frac{\partial}{\partial \eta} \right) v_j^{c,s} \\
&= \mp \frac{j}{r} p_j^{s,c} - \left(1 + \frac{v_0}{r}\right) u_j^{c,s} - \frac{u_0}{r} v^{c,s} \pm \epsilon \left(\frac{2j}{r}\right) u_j^{s,c} \\
&\quad - \left(\xi_r/r \frac{\partial}{\partial \xi}(r \cdot v_0 u_j^{c,s}) \pm \frac{2j}{r} v_0 v_j^{s,c} + \eta_z \frac{\partial}{\partial \eta}(v_0 w_j^{c,s}) \right) + \mathcal{N}^{c,s}(v)_j \,, \qquad \text{(A.7a,b)}
\end{aligned}$$

$$\begin{aligned}
&\frac{\partial}{\partial t} w_j^{c,s} + \xi_r/r \frac{\partial}{\partial \xi}(r \cdot u_0 w_j^{c,s}) + \eta_z \frac{\partial}{\partial \eta}(w_0 w_j^{c,s}) \\
&\quad - \epsilon \left(\xi_r/r \frac{\partial}{\partial \xi} r \xi_r \frac{\partial}{\partial \xi} - \frac{j^2}{r^2} + \eta_z \frac{\partial}{\partial \eta} \eta_z \frac{\partial}{\partial \eta} \right) w_j^{c,s} \\
&= - \eta_z \frac{\partial}{\partial \eta} p_j^{c,s} + \beta T_j^{c,s} - \left(\xi_r/r \frac{\partial}{\partial \xi}(r w_0 u_j^{c,s}) \pm \frac{j}{r}(v_0 w_j^{s,c} + w_0 v_j^{s,c}) \right. \\
&\quad \left. + \eta_z \frac{\partial}{\partial \eta}(w_0 w_j^{c,s}) \right) + \mathcal{N}^{c,s}(w)_j \,, \qquad \text{(A.8a,b)}
\end{aligned}$$

$$\begin{aligned}
&\frac{\partial}{\partial t} T_j^{c,s} + \xi_r/r \frac{\partial}{\partial \xi}(r \cdot u_0 \cdot T_j^{c,s}) + \eta_z \frac{\partial}{\partial \eta}(w_0 T_j^{c,s}) \\
&\quad - \epsilon/\sigma \left(\xi_r/r \frac{\partial}{\partial \xi} r \xi_r \frac{\partial}{\partial \xi} - \frac{j^2}{r^2} + \eta_z \frac{\partial}{\partial \eta} \eta_z \frac{\partial}{\partial \eta} \right) T_j^{c,s} \\
&= - \left(\xi_r/r \frac{\partial}{\partial \xi}(r u_j^{c,s} T_0) \pm \frac{j}{r}(v_0 T_j^{s,c} + v_j^{s,c} T_0) + \frac{\partial}{\partial z}(w_j^{c,s} T_0) \right. \\
&\quad \left. + \mathcal{N}^{c,s}(T)_j \,, \right. \qquad \text{(A.9a,b)}
\end{aligned}$$

$$\xi_r/r \frac{\partial}{\partial \xi}(r u_j^{c,s}) \pm \frac{j v_j^{s,c}}{r} + \eta_z \frac{\partial}{\partial \eta} w_j^{c,s} = 0. \qquad \text{(A.10a,b)}$$

The boundary conditions in (6) and (19) will be formulated in terms of the transformed coordinate in the finite difference form in Appendix B. The diffusive terms in (A.1), (A.6a, b), and (A.7a, b) are written slightly differently in order to form the forcing functions of the pressure equations directly, because some of the differential operators do not commute. It should become clear later.

APPENDIX B: THE FINITE DIFFERENCE EQUATIONS

1. *The Momentum and Pressure Equations*

Equations (A.1)–(A.10) are the complete set of equations for an arbitrary number of waves. When we also allow these waves to assume arbitrary wavenumbers, a little ingenuity will be required to set up a numerical algorithm for $\mathcal{N}$. For only one wave as considered here, we delete the summation sign in (A.1)–(A.4), and set all nonlinear wave–wave interaction terms $\mathcal{N} = 0$ in (A.6)–(A.9).

With these simplifications, and the contracted notations in Eq. (21), the finite difference equations are as follows ($\gamma = \frac{4}{3}$ to maintain $O(\delta t^2)$ accuracy).

$$(\delta_t{}^+u_0)^{\nu+(1/2)} - \epsilon K_z\delta_k(K_z\delta_k u_0)^{\nu+(1/2)} + K_z\delta_k(\overline{u_0}^{K^{\nu+(1/2)}} \cdot \overline{w_0}^{I^\nu})$$
$$= \epsilon(I_r\delta_I(I_r/r\ \delta_I r u_0{}^\nu)) - (2-\gamma)\, I_r/r\ \delta_I(\overline{ru_0}^{I^\nu} \cdot \overline{u_0}^{I^\nu}) - I_r\delta_I p_0^{\nu+(1/2)} + H_1{}^\nu, \quad \text{(A.11a)}$$

$$(\delta_t{}^+u_0)^{\nu+1} - \epsilon(I_r\delta_I(I_r/r\ \delta_I r u_0)^{\nu+1}) + \gamma I_r/r\ \delta_I(\overline{ru_0}^{I^{\nu+1}} \cdot \overline{u_0}^{I^{\nu+(1/2)}})$$
$$= \epsilon K_z\delta_k(K_z\delta_k u_0^{\nu+(1/2)}) - K_z\delta_k(\overline{u_0}^{K^{\nu+(1/2)}} \cdot \overline{w_0}^{I^\nu}) - I_r\delta_I p_0^{\nu+(1/2)} + H_1{}^\nu, \quad \text{(A.11b)}$$

$$H_1{}^\nu = (1 + \overline{v_0}^{I^\nu}/r)\,\overline{v_0}^{I^\nu} - I_r/r\ \delta_I(\overline{ru_j{}^c}^I \cdot \overline{u_j{}^c}^I + \overline{ru_j{}^s}^I \cdot \overline{u_j{}^s}^I)^\nu$$
$$- K_z\delta_k(\overline{u_j{}^c}^K \cdot \overline{w_j{}^c}^I + \overline{u_j{}^s}^K \cdot \overline{w_j{}^s}^I)^\nu + (1/r)((\overline{v_j{}^c}^I)^2 + (\overline{v_j{}^s}^I)^2) \quad \text{(A.11c)}$$

$$(\delta_t{}^+v_0)^{\nu+(1/2)} - \epsilon(I_r\delta_I(I_r/r\ \delta_I r v_0^{\nu+(1/2)})) + I_r/r\ \delta_I(ru_0^{\nu+1} \cdot \overline{v_0}^{I^{\nu+(1/2)}})$$
$$= \epsilon K_z\delta_k(K_z\delta_k v_0{}^\nu) - K_z\delta_k(w_0^{\nu+1} \cdot \overline{v_0}^{K^\nu}) + H_2{}^\nu, \quad \text{(A.12a)}$$

$$(\delta_t{}^+v_0)^{\nu+1} - \epsilon K_z\delta_k(K_z\delta_k v_0^{\nu+1}) + K_z\delta_k(w_0^{\nu+1} \cdot \overline{v_0}^{K^{\nu+1}})$$
$$= \epsilon(I_r\delta_I(I_r/r\ \delta_I r v_0^{\nu+(1/2)})) - I_r/r\ \delta_I(ru_0^{\nu+1} \cdot \overline{v_0}^{I^{\nu+(1/2)}}) + H_2{}^\nu, \quad \text{(A.12b)}$$

$$H_2{}^\nu = -(\overline{u_0}^{I^{\nu+1}} + (\overline{u_0/r}^{I^{\nu+1}}) \cdot v_0{}^\nu) - I_r/r\ \delta_I(ru_j{}^c \cdot \overline{v_j{}^c}^I + ru_j{}^s\,\overline{v_j{}^s}^I)^\nu$$
$$- K_z\delta_k(w_j{}^c \cdot \overline{v_j{}^c}^K + w_j{}^s \cdot \overline{v_j{}^s}^K)^\nu, \quad \text{(A.12c)}$$

$$(\delta_t^+ w_0)^{\nu+(1/2)} - \epsilon(I_r/r\,\delta_I(rI_r\delta_I w_0^{\nu+(1/2)})) + I_r/r\,\delta_I(\overline{ru_0}^{K^{\nu+1}} \cdot \overline{w_0}^{I^{\nu+(1/2)}})$$
$$= \epsilon K_z\delta_k(K_z\delta_k w_0^{\nu}) - (2-\gamma)\,K_z\delta_k(\overline{w_0}^{K^{\nu}}\,\overline{w_0}^{K^{\nu}}) - K_z\delta_k p_0^{\nu+(1/2)} + H_3^{\nu}, \quad \text{(A.13a)}$$

$$(\delta_t^+ w_0)^{\nu+1} - \epsilon K_z\delta_k(K_z\delta_k w_0^{\nu+1}) + \gamma K_z\delta_k(\overline{w_0}^{K^{\nu+1}} \cdot \overline{w_0}^{K^{\nu+(1/2)}})$$
$$= \epsilon(I_r/r\,\delta_I(rI_r\delta_I w^{\nu+(1/2)})) - I_r/r\,\delta_I(\overline{ru_0}^{K^{\nu+1}}\,\overline{w_0}^{I^{\nu+(1/2)}}) - K_z\delta_k p^{\nu+(1/2)} + H_3^{\nu}, \quad \text{(A.13b)}$$

$$H_3^{\nu} = \beta\overline{T}^{K^{\nu}} - I_r/r\,\delta_I(\overline{ru_j^c}^{K} \cdot \overline{w_j^c}^{I} + \overline{ru_j^s}^{K} \cdot \overline{w_j^s}^{I})^{\nu} - K_z\delta_K((\overline{w_j^c}^{K})^2 + (\overline{w_j^s}^{K})^2)^{\nu}. \quad \text{(A.13c)}$$

Since the temperature equations are solved differently, we shall discuss them at the end. The pressure equation is as follows [Eq. (30a)].

$$\nabla^2 p_0^{\nu+(1/2)} = I_r/r\,\delta_I(rRu_0^{\nu}) + K_z\delta_k(Rw_0^{\nu}) + (1 + (\epsilon\Delta t/2)\,\nabla^2(D_0^{\nu}/\Delta t) + 0(\Delta t), \quad \text{(A.14a)}$$

where

$$Ru_0^{\nu} = -I_r/r\,\delta_I(\overline{ru_0}^{I^{\nu}} \cdot \overline{u_0}^{I^{\nu}}) - K_z\delta_k(\overline{u_0}^{K^{\nu}}\,\overline{w_0}^{I^{\nu}}) + H_1^{\nu}, \quad \text{(A.14b)}$$

$$Rw_0^{\nu} = -I_r/r\,\delta_I(\overline{ru_0}^{K^{\nu}} \cdot \overline{w_0}^{I^{\nu}}) - K_z\delta_k(\overline{w_0}^{K^{\nu}} \cdot \overline{w_0}^{K^{\nu}}) + H_3^{\nu}, \quad \text{(A.14c)}$$

$$D_0^{\nu} = I_r/r\,\delta_I(ru_0^{\nu}) + K_z\delta_k w_0^{\nu}. \quad \text{(A.14d)}$$

The boundary conditions will be given after the temperature equations.

The finite difference equations for the amplitude equations are as follows, with $\mathcal{N} = 0$.

$$(\delta_t^+ u_j^{c,s})^{\nu+(1/2)} - \epsilon K_z\delta_k(K_z\delta_k u_j^{c,s})^{\nu+(1/2)} + K_z\delta_k(\overline{w_0}^{I^{\nu+1}} \cdot \overline{u_j^{c,s}}^{K^{\nu+(1/2)}})$$
$$= \epsilon I_r\delta_I(I_r/r\,\delta_I r u_j^{c,s})^{\nu} - I_r/r\,\delta_I(\overline{ru_0}^{I^{\nu+1}} \cdot \overline{u_j^{c,s}}^{I^{\nu}})$$
$$- I_r\delta_I(p_j^{c,s})^{\nu+(1/2)} + (G_{1,j}^{c,s})^{\nu}, \quad \text{(A.15a,b)}$$

$$= \epsilon K_z\delta_k(K_z\delta_k u_j^{c,s})^{\nu+(1/2)} - K_z\delta_k(\overline{w_0}^{I^{\nu+1}} \cdot \overline{u_j^{c,s}}^{K^{\nu+(1/2)}})$$
$$- I_r\delta_I(p_j^{c,s})^{\nu+(1/2)} + (G_{1,j}^{c,s})^{\nu}, \quad \text{(A.15c,d)}$$

$$(G_{1,j}^{c,s})^{\nu} = (1 + (2/r)\,\overline{v_0}^{K^{\nu+1}}) \cdot \overline{v_j^{c,s}}^{K^{\nu}} \pm (2\epsilon j/r)\,\overline{v_j^{s,c}}^{K^{\nu}} + (\epsilon j^2/r^2)\,u_j^{c,s^{\nu}}$$
$$- I_r/r\,\delta_I(\overline{ru_0}^{I^{\nu+1}} \cdot \overline{u_j^{c,s}}^{I^{\nu}}) \pm (j/r)(\overline{v_0}^{I^{\nu+1}} \cdot u_j^{s,c} + u_0^{\nu+1}\,\overline{v_j^{s,c}}^{I^{\nu}})$$
$$+ K_z\delta_k(\overline{u_0}^{K^{\nu+1}} \cdot \overline{w_j^{c,s}}^{I^{\nu}}), \quad \text{(A.15e,f)}$$

$$(\delta_t{}^{+}v_j^{c,s})^{\nu+(1/2)} - \epsilon(I_r\delta_I r I_r\delta_I(v_j^{c,s}/r))^{\nu+(1/2)} + I_r/r\ \delta_I(ru_0^{\nu+1}\ \overline{v_j^{c,s}}^{I})^{\nu+(1/2)}$$

$$= \epsilon(K_z\delta_k K_z\delta_k v_j^{c,s})^{\nu} - K_z\delta_k(w_0^{\nu+1}\ \overline{v_j^{c,s}}^{K})^{\nu} \mp (j/r)(p_j^{s,c})^{\nu+(1/2)} + (G_{2,j}^{c,s})^{\nu}, \quad \text{(A.16a,b)}$$

$$(\delta_t{}^{+}v_j^{c,s})^{\nu+1} - \epsilon(K_z\delta_k K_z\delta_k f_j^{c,s})^{\nu+1} + K_z\delta_k(w_0^{\nu+1}\ \overline{v_j^{c,s}}^{K})^{\nu+1}$$

$$= \epsilon(I_r\delta_I r I_r\delta_I(v_j^{c,s}/r))^{\nu+(1/2)} - I_r/r\ \delta_I(ru_0^{\nu+1}\ \overline{v_j^{c,s}}^{I})^{\nu+(1/2)}$$

$$\mp (j/r)(p_j^{s,c})^{\nu+(1/2)} + (G_{2,j}^{c,s})^{\nu}, \quad \text{(A.16c,d)}$$

$$(G_{2,j}^{c,s})^{\nu} = -(1 + v_0^{\nu+1})\left(\overline{\frac{u_j^{c,s}}{r}}^{I^{\nu+1}}\right) - \left(\overline{\frac{u_0}{r}}^{I^{\nu+1}}\right)\cdot v_j^{c,s^{\nu}} \pm \epsilon\frac{2j}{r}\ \overline{u_j^{s,c}}^{I^{\nu}}$$

$$- \left(I_r/r\ \delta_I(ru_j^{c,s^{\nu}}\ \overline{v_0}^{I})^{\nu+1} \pm \frac{2j}{r}(v_0^{\nu+1}\cdot v_j^{s,c^{\nu}}) + K_z\delta_k(w_{t_j}{}^{s^{\nu}}\ \overline{v_0}^{K})^{\nu+1}\right), \quad \text{(A.16e,f)}$$

$$(\delta_t{}^{+}w_j^{c,s})^{\nu+(1/2)} - \epsilon(I_r/r\ \delta_I r I_r\delta_I w_j^{c,s})^{\nu+(1/2)} + I_r/r\ \delta_I(\overline{ru_0}^{I^{\nu+1}}\ \overline{w_j^{c,s}}^{I^{\nu+(1/2)}})$$

$$= \epsilon K_z\delta_k K_z\delta_k w_j^{c,s^{\nu}} - K_z\delta_k(\overline{w_0}^{K^{\nu+1}}\cdot\overline{w_j^{c,s}}^{K^{\nu}}) - K_z\delta_k(p_j^{c,s})^{\nu+(1/2)} + (G_{3,j}^{c,s})^{\nu}, \quad \text{(A.17a,b)}$$

$$(\delta_t{}^{+}w_j^{c,s})^{\nu+1} - \epsilon K_z\delta_k K_z w_j^{c,s^{\nu+1}} + K_z\delta_k(\overline{w_0}^{K^{\nu+1}}\cdot\overline{w_j^{c,s}}^{K^{\nu+1}})$$

$$= \epsilon(I_r/r\ \delta_I r I_r\delta_I w_j^{c,s})^{\nu+(1/2)} - I_r/r\ \delta_I(\overline{ru_0}^{K^{\nu+1}}\cdot\overline{w_j^{c,s}}^{\nu+(1/2)})$$

$$- K_z\delta_k(p_j^{c,s})^{\nu+(1/2)} + (G_{3,j}^{c,s})^{\nu}, \quad \text{(A.17c,d)}$$

$$(G_{3,j}^{c,s})^{\nu} = -(\epsilon j^2/r^2)\ w_j^{c,s^{\nu}} + \beta\ \overline{T_j^{c,s}}^{K^{\nu}} - (I_r/r\ \delta_I(\overline{ru_j^{c,s}}^{K^{\nu+1}}\cdot\overline{w_0}^{I^{\nu+1}})$$

$$\pm (j/r)(\overline{v_0}^{K^{\nu+1}}\cdot w_j^{s,c^{\nu}} + w_0\ \overline{v_j^{s,c}}^{K^{\nu+1}}) + K_z\delta_k(\overline{w_0}^{K^{\nu+1}}\cdot\overline{w_j^{c,s}}^{K^{\nu}})), \quad \text{(A.17e,f)}$$

$$\hat{\nabla}_j{}^2 p_j^{c,s^{\nu+(1/2)}} = e_j^{c,s^{\nu+(1/2)}}, \quad \text{(A.18a,b)}$$

where

$$\hat{\nabla}_j{}^2 = (I_r/r\ \delta_I r I_r\delta_I + K_z\delta_k K_z\delta_k - (j^2/r^2)), \quad \text{(A.18c)}$$

$$e_j^{c,s^{\nu+(1/2)}} = (1/\delta t)\ D_j^{c,s^{\nu}} + (\epsilon/2)\ \nabla^2 D_j^{c,s^{\nu}} + I_r/r\ \delta_I r(G_{1,j}^{c,s^{\nu}} - H_{1,j}^{*c,s^{\nu}})$$

$$\mp (j/r)(G_{2,j}^{s,c^{\nu}} - H_{2,j}^{*c,s^{\nu}}) + K_z\delta_k(G_{3,j}^{c,s^{\nu}} - H_{3,j}^{*c,s^{\nu}}), \quad \text{(A.19a,b)}$$

$$D_j^{c,s^{\nu}} = (I_r/r\ \delta_I r u_j^{c,s^{\nu}} \pm (j/r)\ v_j^{s,c^{\nu}} + K_z\delta_k w_j^{c,s^{\nu}}), \quad \text{(A.19c,d)}$$

$$\nabla^2 = (I_r/r\ \delta_I r I_r\delta_I + K_z\delta_k K_z\delta_k), \quad \text{(A.19e)}$$

$$H_{1,j}^{*c,s\nu} = I_r/r\ \delta_I(\overline{ru_0}^{I^{\nu+1}} \cdot \overline{u_j^{c,s}}^{I^{\nu}}) + K_z\delta_k(\overline{w_0}^{I^{\nu+1}} \cdot \overline{u_j^{c,s}}^{K^{\nu}}), \qquad \text{(A.20a,b)}$$

$$H_{2,j}^{*c,s\nu} = I_r/r\ \delta_I(ru_0^{\nu+1}\ \overline{v_j^{c,s}}^{I^{\nu}}) + K_z\delta_k(w_0^{\nu+1}\ \overline{v_j^{c,s}}^{K}), \qquad \text{(A.20c,d)}$$

$$H_{3,j}^{*c,s\nu} = I_r/r\ \delta_I(\overline{ru_0}^{K^{\nu+1}}\ \overline{w_j^{c,s}}^{I}) + K_z\delta_k(\overline{w_0}^{I^{\nu+1}} \cdot \overline{w_j^{c,s}}^{K^{\nu}}). \qquad \text{(A.20e,f)}$$

2. *The Temperature Equations*

Formally, Eq. (A.4) can be written as follows in terms of spatial finite differences [with the summation sign deleted from (A.4)].

$$(\partial/\partial t)\ T_0 + I_r/r\delta_I(ru_0T_0) + K_z\delta_k(w_0T_0) - (\epsilon/\sigma)(I_r/r\delta_I(rI_r\delta_I) + K_z\delta_kK_z\delta_k)\ T_0$$
$$= -I_r/r\delta_I(ru_j^cT_j^c + ru_j^sT_j^s) - K_z\delta_k(w_j^cT_j^c + w_j^sT_j^s). \qquad \text{(A.21)}$$

Multiply (A.21) by (r/I_rK_z) and define $\Gamma = rT/I_rK_z$, $U = ru$, $W = rw$. We have

$$(\partial/\partial t)\ \Gamma_0 + \delta_I[U_0(\Gamma_0I_r/r)] + \delta_k[W_0(\Gamma_0K_z/r)]$$
$$- (\epsilon/\sigma)(r\delta_I(I_r/r)\ \delta_I(\Gamma_0I_r) + \Gamma_0/r^2 + \delta_kK_z\delta_k(\Gamma_0K_z)) = H_4^{\nu}, \qquad \text{(A.22a)}$$

where

$$H_4^{\nu} = -\delta_I[U_j^c(\Gamma_j^cI_r/r) + U_j^s(\Gamma_j^sI_r/r)] - \delta_k[W_j^c(\Gamma_j^cK_z/r) + W_j^s(\Gamma_j^sK_z/r)]. \qquad \text{(A.22b)}$$

Equation (A.22a) is solved by fractional time steps [17].

$$\hat{\delta}_t\Gamma_0^* + \delta_I^*[U_0(\Gamma_0I_r/r)] = 0, \qquad \text{(A.23a)}$$

$$\hat{\delta}_t\Gamma_0^{**} + \delta_k^{**}[W_0(\Gamma_0K_z/r) = 0, \qquad \text{(A.23b)}$$

$$\hat{\delta}_t\Gamma_0^{***} - (\epsilon/\sigma)(r\delta_I(I_r/r)\ \delta_I(\Gamma_0^{***}I_r) + \Gamma_0^{***}/r^2)$$
$$= (\epsilon/\sigma)(\delta_kK_z\delta_k(\Gamma_0^{**}K_z)) + H_4^{\nu}, \qquad \text{(A.23c)}$$

$$\hat{\delta}_t\Gamma_0^{****} - (\epsilon/\sigma)(\delta_kK_z\delta_k(\Gamma_0^{****}K_z))$$
$$= (\epsilon/\sigma)(r\delta_I(I_r/r)\ \delta_I(\Gamma_0^{***}I_r) + \Gamma_0^{***}/r^2) + H_4^{\nu}. \qquad \text{(A.23d)}$$

Equations (A.23a) and (A.23b) are further solved by fractional steps simultaneously in two opposite directions as follows.

$$\left.\begin{aligned} &\hat{\delta}_t\Gamma_{0i}^{(1)} + \vec{\delta}_I(U_0^{\nu+1}\Gamma_0I_r/r)_i^{(1)} = 0, \qquad i = 2,\ldots, L/2, \\ &\hat{\delta}_t\Gamma_{0i}^{(1)} + \overleftarrow{\delta}_I(U_0^{\nu+1}\Gamma_0I_r/r)_i^{(1)} = 0, \qquad i = L-1,\ldots, L/2+1, \end{aligned}\right\} \text{simultaneous operation} \qquad \text{(A.24a,b)}$$

$$\left.\begin{aligned} \hat{\delta}_t \Gamma_{0i}^{(2)} + \vec{\delta}_I (U_0^{\nu+1} \Gamma_0 I_r / r)_i^{(2)} &= 0, \qquad i = L/2 + 1, \ldots, L - 1, \\ \hat{\delta}_t \Gamma_{0i}^{(2)} + \overleftarrow{\delta}_I (U_0^{\nu+1} \Gamma_0 I_r / r)_i^{(2)} &= 0, \qquad i = L/2, \ldots, 2, \end{aligned}\right\} \text{ simultaneous operation} \quad \text{(A.25a,b)}$$

$$\left.\begin{aligned} \hat{\delta}_t \Gamma_{0k}^{(3)} + \vec{\delta}_k (W_0^{\nu+1} \Gamma_0 K_z / r)_k^{(3)} &= 0, \qquad k = 2, \ldots, N/2, \\ \hat{\delta}_t \Gamma_{0k}^{(3)} + \overleftarrow{\delta}_k (W_0^{\nu+1} \Gamma_0 K_z / r)_k^{(3)} &= 0, \qquad k = N - 1, \ldots, N/2 + 1, \end{aligned}\right\} \text{ simultaneous operation} \quad \text{(A.26a,b)}$$

$$\left.\begin{aligned} \hat{\delta}_t \Gamma_{0i}^{(4)} + \vec{\delta}_k (W_0^{\nu+1} \Gamma_0 K_z / r)_k^{(4)} &= 0, \qquad k = N/2 + 1, \ldots, N - 1, \\ \hat{\delta}_t \Gamma_{0k}^{(4)} + \overleftarrow{\delta}_k (W_0^{\nu+1} \Gamma_0 K_z / r)_k^{(4)} &= 0, \qquad k = N/2, \ldots, 2, \end{aligned}\right\} \text{ s}^1\text{mu}_3\text{taneous operat}^1\text{on} \quad \text{(A.27a,b)}$$

where $\hat{\delta}_t$, $\vec{\delta}$, and $\overleftarrow{\delta}$ are defined as

$$\begin{aligned} \hat{\delta}_t f^{(\alpha)} &= (f^{(\alpha)} - f^{(\alpha-1)})/(\Delta t/2), \\ \vec{\delta}_\lambda (\phi f)^{(\alpha)} &= (\phi_{\lambda+(1/2)} f_{\lambda+1}^{(\alpha-1)} - \phi_{\lambda-(1/2)} f_{\lambda-1}^{(\alpha)})/2, \\ \overleftarrow{\delta}_\lambda (\phi f)^{(\alpha)} &= (\phi_{\lambda+(1/2)} f_{\lambda+1}^{(\alpha)} - \phi_{\lambda-(1/2)} f_{\lambda-1}^{(\alpha-1)})/2. \end{aligned} \quad \text{(A.28a,b,c)}$$

The operations in (A.28b, c) are similar to those discussed by Piacsek and Williams [16]. We found it necessary to operate from both directions simultaneously in order to retain symmetry in test runs with $r_0 \to \infty$. This operation imposes a small constraint, i.e. the number of gridpoints must be even.

Equations (A.23c) and (A.23d) are solved by the usual ADI procedure, with the two, three, and four stars replaced by superscripts (4), (6), and (8), and define

$$\hat{\delta}_t \Gamma_0^{(6)} = (\Gamma^{(6)} - \Gamma^{(4)})/(\Delta t/2), \; \hat{\delta}_t \Gamma_0^{(8)} = (\Gamma^{(8)} - \Gamma^{(6)})/(\Delta t/2). \quad \text{(A.29)}$$

If we add up Eqs. (A.24)–(A.27), (A.23c), and (A.23d), we have

$$\begin{aligned} &(\Gamma_0^{(8)} - \Gamma^{(0)})/\Delta t \\ &\quad = -\tfrac{1}{2}(\delta_I (U_0^{\nu+1} \Gamma_0)^{(1)} + \delta_I (U_0^{\nu+1} \Gamma_0)^{(2)}) - \tfrac{1}{2}(\delta_k (W_0^{\nu+1} \Gamma_0)^{(3)} + \delta_k (W_0^{\nu+1} \Gamma_0)^{(4)}) \\ &\qquad + (\epsilon/\sigma)(r \delta_I (I_r/r)\, \delta_I (\Gamma_0^{(6)} I_r) + \Gamma_0^{(6)}/r^2) + (\epsilon/\sigma)(\delta_k K_z \delta_k ((\Gamma_0^{(4)} + \Gamma_0^{(8)})/2) \cdot K_z) \\ &\qquad + H_4^\nu, \end{aligned} \quad \text{(A.30)}$$

where $\Gamma_0^{(0)} = \Gamma_0^\nu$, $\Gamma_0^{(8)} = \Gamma_0^{\nu+1}$. The different terms on the right-hand side are evaluated at different times within a time step as the fractional time-step method normally requires.

Equations (A.9a, b) are solved in a similar manner. If we define $\Gamma_j^{c,s} = (rT_j^{c,s})/(I_r K_z)$, we have

$$(\partial/\partial t)\,\Gamma_j^{c,s} + \delta_I[U_0(\Gamma_j^{c,s} I_r/r)] + \delta_k[W_0(\Gamma_j^{c,s} K_z/r)]$$
$$- (\epsilon/\sigma)(r\delta_I(I_r/r)\,\delta_I(\Gamma_j^{c,s} I_r) + \Gamma_j^{c,s}/r^2 - (j^2/r^2)\,\Gamma_j^{c,s} + \delta_k K_z \delta_k(\Gamma_j^{c,s} K_z))$$
$$= (G_{4,j}^{c,s})^\nu, \qquad \text{(A.31a,b)}$$

where

$$(G_{4,j}^{c,s})^\nu = -\{\delta_I[U_j^{c,s^{\nu+1}}(\Gamma_0^{\nu+1} I_r/r)] \pm (j/r)(v_0^{\nu+1}\Gamma_j^{s,c^\nu} + v_j^{s,c^{\nu+1}}\Gamma_0^{\nu+1})$$
$$+ \delta_k[W_j^{c,s^{\nu+1}}(\Gamma_0^{\nu+1} K_z/r)]\}. \qquad \text{(A.31c,d)}$$

Equations (A.31a, b) are solved by fractional steps as follows.

$$\delta_t \Gamma_j^{c,s^{(1)}} + \overrightarrow{\delta}_I[U_0^{\nu+1}(\Gamma_j^{c,s} I_r/r)]^{(1)} = 0, \qquad \begin{matrix} i = 2,\ldots, L/2, \\ i = L-1,\ldots, L/2+1, \end{matrix}$$

$$\delta_t \Gamma_j^{c,s^{(2)}} + \overleftarrow{\delta}_I[U_0^{\nu+1}(\Gamma_j^{c,s} I_r/r)]^{(2)} = 0, \qquad \begin{matrix} i = L/2+1,\ldots, L-1, \\ i = L/2,\ldots, 2, \end{matrix}$$

$$\delta_t \Gamma_j^{c,s^{(3)}} + \overrightarrow{\delta}_k[W_0^{\nu+1}(\Gamma_j^{c,s} K_z/r)]^{(3)} = 0, \qquad \begin{matrix} k = 2,\ldots, N/2, \\ k = N-1,\ldots, N/2+1, \end{matrix}$$

$$\delta_t \Gamma_j^{c,s^{(4)}} + \overleftarrow{\delta}_k[W_0^{\nu+1}(\Gamma_j^{c,s} K_z/r)]^{(4)} = 0, \qquad \begin{matrix} k = N/2+1,\ldots, L-1, \\ k = N/2,\ldots, 2, \end{matrix}$$

where $\overrightarrow{\delta}$ denotes two separate steps as before, but the operation is simultaneous. The rest of Equations (A.31) are solved by ADI:

$$\delta_t^{(6)} \Gamma_j^{c,s} - (\epsilon/\sigma)(r\delta_I(I_r/r)\,\delta_I(\Gamma_j^{c,s^{(6)}} I_r) + \Gamma_j^{c,s^{(6)}}/r^2 - (j^2/r^2)\,\Gamma_j^{c,s^{(6)}})$$
$$= (\epsilon/\sigma)(\delta_k K_z \delta_k(\Gamma_j^{c,s^{(4)}} K_z)) + (G_{4,j}^{c,s})^\nu,$$

$$\delta_t^{(8)} \Gamma_j^{c,s} - (\epsilon/\sigma)(\delta_k K_z \delta_k(\Gamma_j^{c,s^{(8)}} K_z))$$
$$= (\epsilon/\sigma)(r\delta_I(I_r/r)\,\delta_I(\Gamma_j^{c,s^{(6)}} I_r) + \Gamma_j^{c,s^{(6)}}/r^2 - (j^2/r^2)\,\Gamma_j^{c,s^{(6)}}) + (G_{4,j}^{c,s})^\nu,$$

where

$$(G_{4,j}^{\alpha,s})_{ik}^\nu = -\{[(U_j^{c,s^{\nu+1}})_{i+(1/2),k} \cdot (\Gamma_0^{\nu+1} I_r/r)_{i+1,k} - (U_j^{c,s})_{i-(1/2),k}$$
$$\cdot (\Gamma_0^{\nu+1} I_r/r)_{i-1}] \pm (j/r)(v_0^{\nu+1}\Gamma_j^{s,c^\nu} + v_j^{s,c^{\nu+1}}\Gamma_0^{\nu+1})$$
$$+ \delta_k[(W_j^{c,s^{\nu+1}})_{ik+(1/2)} \cdot (\Gamma_0^{\nu+1} K_z/r)_{ik+1} - (W_i^{c,s^{\nu+1}})_{ik-(1/2)} \cdot (\Gamma_0^{\nu+1} K_z/r)_{ik-1}]\}.$$

3. *Boundary Conditions*

Equations (6) and (19) show that the boundary conditions require either that the function itself be specified, $\phi_0 = f_1$ (the Dirichlet condition), or that its normal derivative be specified, $(\partial\phi/\partial n)_0 = f_2$ (the Neumann condition), on the boundaries.

For boundaries at, say, $i = 0$, between two grid points at $i = \pm\frac{1}{2}$, as those of v, t, p on all boundaries, those of u on the horizontal boundaries and those of w on the vertical boundaries, the approximation is as follows.

$$\text{Dirichlet condition:} \quad (\phi_{1/2} + \phi_{-1/2})/2 = f_1\,, \qquad \phi_{-1/2} = 2f_1 - \phi_{1/2}\,,$$

$$\text{Neumann condition:} \quad (\phi_{1/2} - \phi_{-1/2}) = f_2\,, \qquad \phi_{-1/2} = \phi_{1/2} - f_2\,.$$

When the boundary coincides with the grid points, such as those of u on the vertical boundaries and those of w on the horizontal boundaries, the Dirichlet condition requires $\phi_0 = f_1$. No Neumann condition is applied to grid points right on the boundaries in our grid system.

4. *Iteration Procedure*

All equations (except the advective parts of the temperature equations) are iterated semi-implicitly in the horizontal, and then the vertical, direction (or vice versa) to form one time step. The unknowns at three adjacent grid points are related by

$$-A_l\phi_{l-1} + B_l\phi_l - C_l\phi_{l+1} = D_l\,.$$

All unknowns on each line are related by the matrix equation

$$A\phi = Q,$$

where A is a tridiagonal $M \times M$ matrix, ϕ a column matrix, and Q a row matrix, each containing M elements. The matrix A can be easily inverted with Gaussian elimination to solve for ϕ. For a detailed description of the standard ADI technique, see [22, p. 209, 1962].

It is important to note that we have included on the left-hand side the advective terms of the momentum equations. If these terms are large in comparison with the diffusion term such that the diagonal elements are no longer dominant, the standard ADI method used here will no longer be efficient. For this reason, we have to solve the temperature equations slightly differently. For some parameters, the advection of temperature is the dominant transport mechanism in some parts of the fluid. If we had used ADI for the whole temperature equation, we would have to iterate a large number of times for convergence. In fact, there is no guarantee that convergence could be obtained for the highly nonlinear region of the fluid.

5. *The Overall Order of Iteration*

The order in which we iterate the equations is

$$\begin{array}{l} u_0 \rightarrow w_0 \rightarrow v_0 \\ \uparrow \qquad\qquad\quad \downarrow \\ \text{——} p_0 \rightarrow t_0 \end{array}$$

to obtain an advanced axisymmetric field for each of the zero subscripted variables. Then introduce random field $O(10^{-2})$ as perturbation for T^c and T^s, and iterate the whole set of equations as follows.

$$\begin{array}{l} u_0 \rightarrow w_0 \rightarrow v_0 \rightarrow T_0 \rightarrow u^c \rightarrow u^s \rightarrow v^c \rightarrow v^s \\ \uparrow \qquad\qquad\qquad\qquad\qquad\qquad\qquad\qquad\qquad\qquad\quad \downarrow \\ \text{——} p^s \leftarrow p^c \leftarrow p_0 \leftarrow T^s \leftarrow T^c \leftarrow w^s \leftarrow w^c. \end{array}$$

6. *Conservation of Quadratics*

In the absence of dissipation, it can be shown that the present algorithm conserves the quadratics of every field. Except for a slight displacement in time, the quadratics of temperature are conserved by straight summation over the spatial domain of integration [16]. So is the kinetic energy due to Coriolis and centrifugal terms. If these are called unconditional conservation, the conservation of kinetic energy (the quadratics of momentum) is conditional. The condition is $\nabla \cdot \mathbf{V} \equiv 0$ in finite difference form.

It is too tedious to write down the quadratic form of all the equations. The quadratic conservation is equivalent to the time invariant of the kinetic energy and temperature square as follows.

$$(\partial/\partial t) \int (u_0^2 + v_0^2 + w_0^2 + u_j^{c^2} + u_j^{s^2} + v_j^{c^2} + v_j^{s^2} + w_j^{c^2} + w_j^{s^2})\, r\, dr\, dz = 0,$$

$$(\partial/\partial t) \int (T_0^2 + T_j^{c^2} + T_j^{s^2})\, r\, dr\, dz = 0.$$

7. *Further Development*

It is worth mentioning that the algorithm for the temperature equation reported here is only one of the many possible combinations of fractional time steps and ADI methods. This particular one is reported here because the results of this paper

The results will be reported in the future.

ACKNOWLEDGMENTS

This work was done at the Geophysical Fluid Dynamics Institute, Florida State University, upon the invitation of Professor Pfeffer, to whom the author owes not only the rare opportunity to tackle this complex scientific problem freely, but also 20 months' beautiful Florida sunshine. Professor Pfeffer initiated the problem and suggested the semispectral and variable grid approach. His intimacy with the laboratory experimental results provided the needed insight and encouragement on more than one occasion. Mr. James Zarichny's expert computer programming relieved the author of much of the routine drudgery that writing a large computer program always requires. His cheerful cooperation and hard work is hereby gratefully acknowledged. The author has also benefited immensely from discussions with Drs. Blumsack, O'Brien, and Wessel and other members of *GFDI*, who made the author's visit more than pleasant. Dr. Warn-Varnas of NRL provided the NRL Poisson solver package which we modified and used. I also thank the Director of Bedford Institute for his consent to my leave of absence.

The research was supported by ONR contract N00014-68-A-0159. The computations were done on the CDC 6500 at Florida State University, and the computer plots were done on the CDC 6600 at NCAR. Both computer facilities are supported by the National Science Foundation.

REFERENCES

1. R. C. BEARDSLEY, *J. Computational Phys.* **7** (1971), 273–288.
2. D. E. DIETRICH, *Pure Appl. Geophys.* **109** (1973), 1826–1861.
3. E. T. EADY, *Tellus* **1** (1949), 33–52.
4. E. ELIASEN, B. MACHENHAUER, AND E. RASMUSSEN, On a numerical Method for Integration of the Hydrodynamical Equations with a Spectral Representation of the Horizontal Fields. Report No. 2, Københavns Universitet, Institut for Teoretic Meteorologi, Copenhagen, Denmark, 1970.
5. D. FULTZ *et al.*, "Studies of Thermal Convection in a Rotating Cylinder with Some Implication for Large-Scale Atmospheric Motions," *Meteorological Monograph* **4** (21), American Meteorological Society, 1959.
6. P. A. GILMAN, *Solar Phys.* **27** (1972), 3–26.
7. F. H. HARLOW AND J. E. WELCH, *Phys. Fluids* **8** (1965), 2128–2189.
8. R. HIDE, *Philos. Trans. Roy. Soc. London, Ser. A* **250** (1958), 441–478.
9. E. KALNAY DE RIVAS, *J. Computational Phys.* **10** (1972), 202–210.
10. H. O. KREISS AND J. OLIGER, *Tellus* **24** (1972), 199–215.
11. B. MACHENHAUER AND E. RASMUSSEN, On the Integration of the Spectral Hydrodynamical Equations by a Transform Method, Report No. 3, Københavns Universitet, Institut for Teorectic Meteorologi, Copenhagen, Denmark, 1972.
12. N. A. MCFARLANE, Axisymmetric Flow and Stability in the Lower Symmetry Regine of a Differentially Heated Rotating Annulus of Fluid. Ph.D. Thesis, University of Michigan, 1974.
13. S. A. ORSZAG, *J. Atmos. Sci.* **27** (1970), 890–895.
14. S. A. ORSZAG, *Stud. Appl. Math.* **1** (1971), 293–327.
15. R. PFEFFER, G. BUZYNA, AND W. W. FOWLIS, *J. Atmos. Sci.* **31** (1974), 622–645.
16. S. A. PIACSEK AND G. P. WILLIAMS, *J. Computational Phys.* **6** (1970), 392–405.
17. R. D. RICHTMYER AND K. W. MORTON, "Difference Method for Initial Value Problems," Interscience, New York, 1967.

18. G. O. ROBERTS, Computational Meshes for Boundary Layer Problems, in "Proceedings of the Second International Conference on Numerical Methods in Fluid Dynamics" (M. Holt., Ed.), pp. 171–177, Springer–Verlag, Berlin/Heidelberg/New York, 1971.
19. K. V. ROBERTS AND N. O. WEISS, *Math. Comp.* **20** (1966), 272–299.
20. M. SUNDQVIST AND G. VERONIS, *Tellus* **22** (1970), 26–31.
21. P. N. SWARTZTRAUBER, *SIAM J. Numerical Analysis* **11** (1974), 1136–1150.
22. R. S. VARGA, "Matrix Iterative Analysis," Prentice–Hall, Englewood Cliffs, N.J., 1962.
23. G. P. WILLIAMS, *J. Fluid Mech.* **37** (1969), 727–750.
24. G. P. WILLIAMS, *J. Fluid Mech.* **49** (1971), 417–449.